WEST COAST REGIONAL CARBON SEQUESTRATION PARTNERSHIP - REPORT ON GEOPHYSICAL TECHNIQUES FOR MONITORING CO_2 MOVEMENT DURING SEQUESTRATION

FINAL REPORT

Erika Gasperikova[1]

G. Michael Hoversten[2]

Lawrence Berkeley National Laboratory

One Cyclotron Rd

Mail Stop 90-1116

Berkeley CA, 94720

October 2005

EGasperikova@lbl.gov [1]

gmhoversten@lbl.gov [2]

DISCLAIMER

CONTENTS

LIST OF FIGURES

Abstract

The relative merits of the seismic, gravity, and electromagnetic (EM) geophysical techniques are examined as monitoring tools for geologic sequestration of CO_2. This work does not represent an exhaustive study, but rather demonstrates the capabilities of a number of geophysical techniques on two synthetic modeling scenarios. The first scenario represents combined CO_2 enhance oil recovery (EOR) and sequestration in a producing oil field, the Schrader Bluff field on the north slope of Alaska, USA. EOR/sequestration projects in general and Schrader Bluff in particular represent relatively thin injection intervals with multiple fluid components (oil, hydrocarbon gas, brine, and CO_2). This model represents the most difficult end member of a complex spectrum of possible sequestration scenarios. The time-lapse performance of seismic, gravity, and EM techniques are considered for the Schrader Bluff model. The second scenario is a gas field that in general resembles conditions of Rio Vista reservoir in the Sacramento Basin of California. Surface gravity, and seismic measurements are considered for this model.

Executive Summary

This report considers the application of a number of different geophysical techniques for monitoring geologic sequestration of CO_2. The relative merits of seismic, gravity, and electromagnetic are considered for monitoring. Numerical modeling has been done on flow simulations based on a proposed CO_2 sequestration project in the Schrader Bluff field on the North Slope of Alaska as well as a gas field that in general resembles conditions of Rio Vista reservoir in the Sacramento Basin of California.

The time-lapse performance of seismic, gravity, and EM techniques are considered for the Schrader Bluff model. This model represents the most difficult end member of a complex spectrum of possible sequestration scenarios because of thin injection intervals with multiple fluid components (oil, hydrocarbon gas, brine, and CO_2). The spatial variations in the changes in the vertical component of gravity as well as the vertical gradient of the vertical component of gravity directly correlate with the spatial variations in the net density changes within the reservoir. Although the magnitude of the signals measured on the surface is in the noise level of the field survey, borehole measurements just above the reservoir do produce measurable change in the vertical component of gravity that could be used to map lateral distributions of injected CO_2. The difference in both the borehole gravity response and the vertical gravity gradient measured in vertical profiles within boreholes clearly identifies the position of the reservoir. There is a clear change in seismic amplitude associated with the reservoir caused by the changes is water and CO_2 saturation. In addition, there is a change in the seismic AVO effects. Both seismic amplitude and AVO can be exploited to make quantitative estimates of saturation changes. There is a direct one-to-one correspondence with the change in S_w and the change in the electric field amplitude. While this signal level is low, it can be measured give the signal-to-noise ratio of the data. While this represents a potential low-cost monitoring technique it is best suited for CO_2 – brine systems where there is a one-to-one correlation between the change in water saturation and the change in CO_2 saturation (since $S_w + S_{CO2} = 1$). In petroleum reservoir such as Schrader Bluff the presence of hydrocarbon as additional fluids eliminates the one-to-one correlation between changes in S_w and changes in S_{CO2}.

The seismic and gravity responses were simulated for a simplified flow simulation model of the Rio Vista gas field in Sacramento Basin, California. Models were used to calculate anticipated contrasts in seismic velocity, density and impedance in gas-saturated rock when CO_2 is introduced. Numerical simulations were performed to evaluate whether a CO_2-CH_4 front can be monitored using seismic and/or gravity. For the gas field used in this study, the change in reservoir properties are very small and neither gravity nor seismic methods would provide information necessary for monitoring of CO_2 movement.

Introduction

Petroleum reservoirs are the most obvious sequestration targets. Petroleum reservoirs have the natural advantages that they are already well characterized, have a demonstrated seal, have an existing infrastructure, and offer cost offsets in the form of enhanced petroleum production as CO_2 is injected. From a monitoring standpoint, petroleum reservoirs offer more challenges than for brine formations because they typically have less vertical extent (~25m for oil vs. 100's of m for brine formations) and have multiple in-situ fluids. Not withstanding their inherent monitoring challenges, petroleum reservoir will undoubtedly provide many of the early sequestration examples.

Candidate sites for geologic sequestration included Elk Hills, California (Occidental), Ventura, California (Aera), and Schrader Bluff, Alaska (BP). Occidental decided not to participate in this study, Ventura didn't have an existing reservoir model and available information wasn't enough to create one. Since depleted gas reservoirs are another candidate for CO_2 sequestration, we included the study of Rio Vista gas field in Sacramento Basin, California. This report provides an evaluation of several geophysical monitoring techniques. This analysis makes use of realistic scenarios for a combined enhanced oil/gas recovery (EOR/EGR) and CO_2 storage project. It is based on the Schrader Bluff oil field on the North Slope of Alaska and the Rio Vista gas field in Sacramento Basin, California.

On-shore EOR project – Schrader Bluff, Alaska

A joint industry project comprising BP, ChevronTexaco, Norsk Hydro, Shell, Statoil, Suncor was formed with the goal of developing technologies to enable the cost effective CO_2 capture and sequestration. One site being considered is the Schrader Bluff reservoir

on Alaska's North Slope (Figure 1). Preliminary evaluations show that a CO_2 based enhanced oil recovery could increase oil recovery by up to 50% over waterflooding (Hill et al, 2000). Furthermore, the studies concluded that up to 60% of the CO_2 injected as part of the EOR scheme would remain in the reservoir. A schematic geological cross-section through the Schrader Bluff Formation is shown in Figure 2.

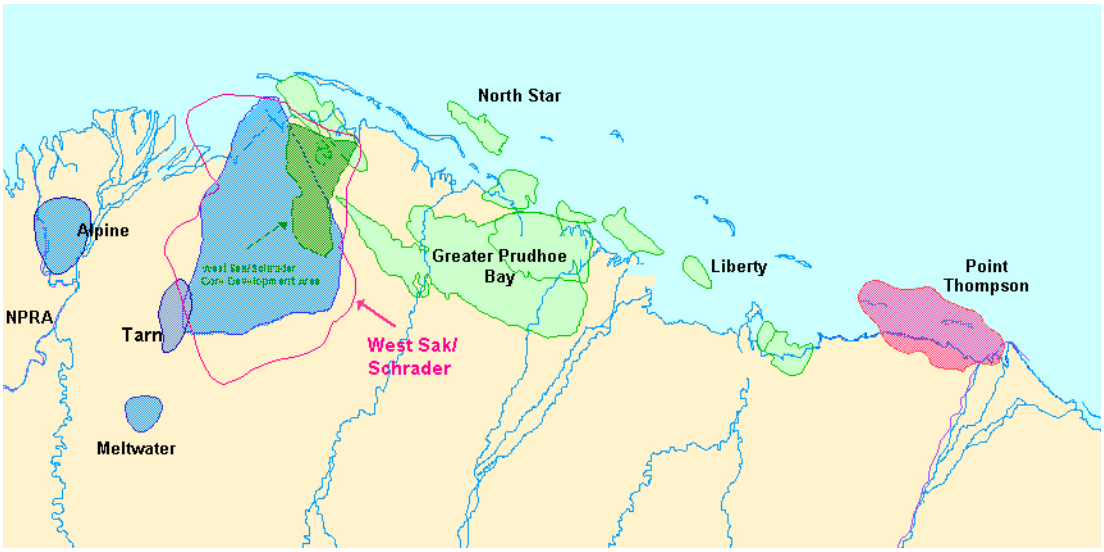

Figure 1: Location of Schrader Bluff reservoir on Alaska's North Slope.

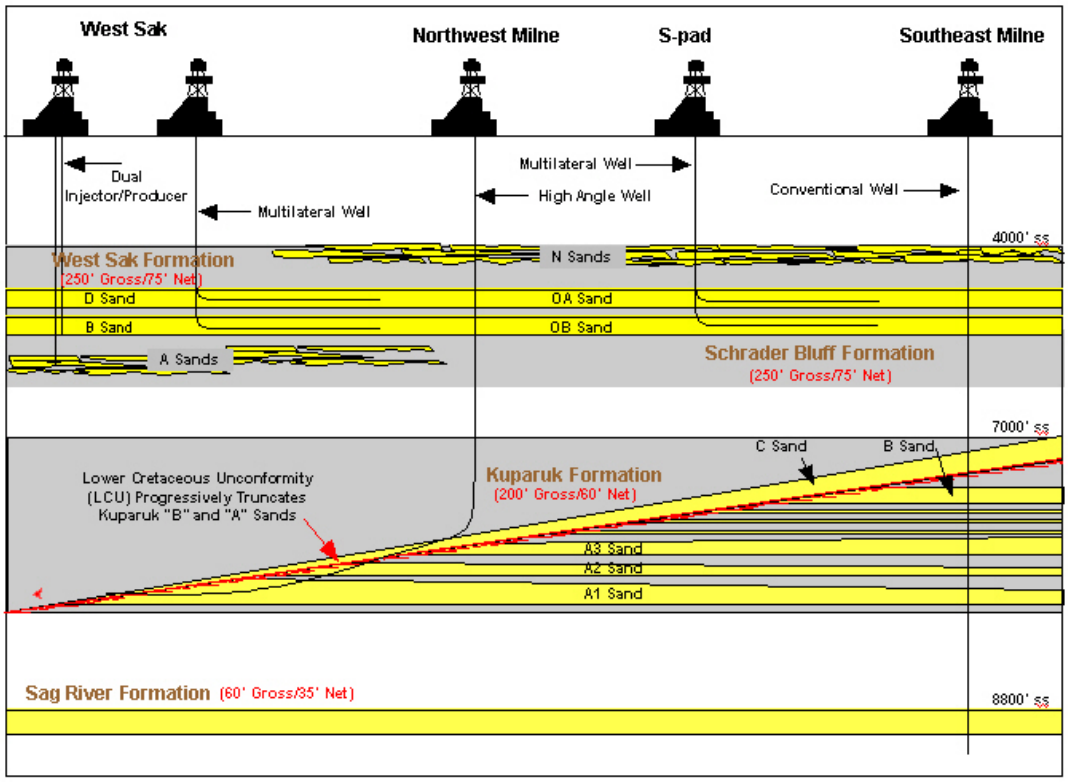

Figure 2: A schematic geological cross-section through the Schrader Bluff Formation.

In order to compare the spatial resolution and sensitivity of various geophysical techniques being considered for CO_2 sequestration monitoring a three-dimensional (3D) flow simulation model the reservoir provided by BP was used in conjunction with rock-properties relations developed from log data to produce geophysical models from the flow simulations. The Schrader Bluff reservoir is a sandstone unit, between 25 and 30 m thick, at a depth of 1,100 – 1,400 m. Figure 3 shows a 3-D view of the portion of the reservoir under consideration for a CO_2 sequestration test. The reservoir unit gently dips to the east with major faulting running mainly north-south. Two faults with offsets in excess of 75 m cut the reservoir with several smaller sub-parallel faults present. Time-lapse snap shots of the reservoir at initial conditions and 5-year increments out to 2035 were used. A water after gas (WAG) injection strategy is considered which produces complicated spatial variations in both CO_2 and water saturation within the reservoir over time.

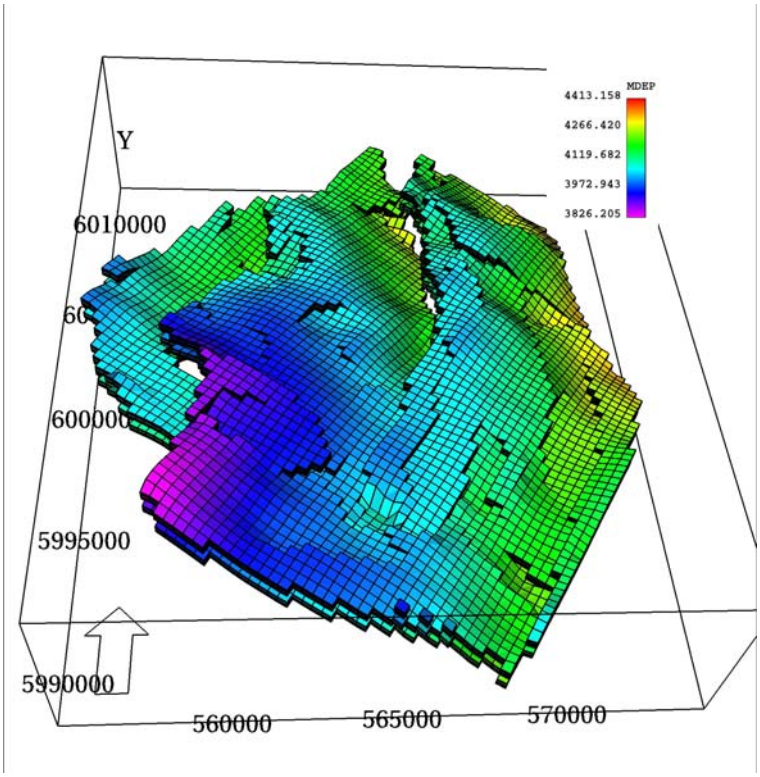

Figure 3. Three-dimensional view of the portion of the reservoir under consideration for CO2 sequestration test at Schrader Bluff. Depths range between 3,800 and 4,400 feet (1,158 and 1,341 m) true vertical depth.

Rock Properties Model

Rock properties models were developed from log data for the reservoir. These models relate reservoir parameters to geophysical parameters and are used to convert the flow simulation model parameters to geophysical parameters (V_P, V_S, density and electrical resistivity). A description of the rock-properties modeling process is given by Hoversten et al. (2003). Electrical resistivity as a function of porosity and water saturation using an Archie's law formulation is used. Seismic properties are modeled as shown in Figure 4. The predicted V_p, V_s and density from the derived model based on log data from the MSP-15 well are shown.

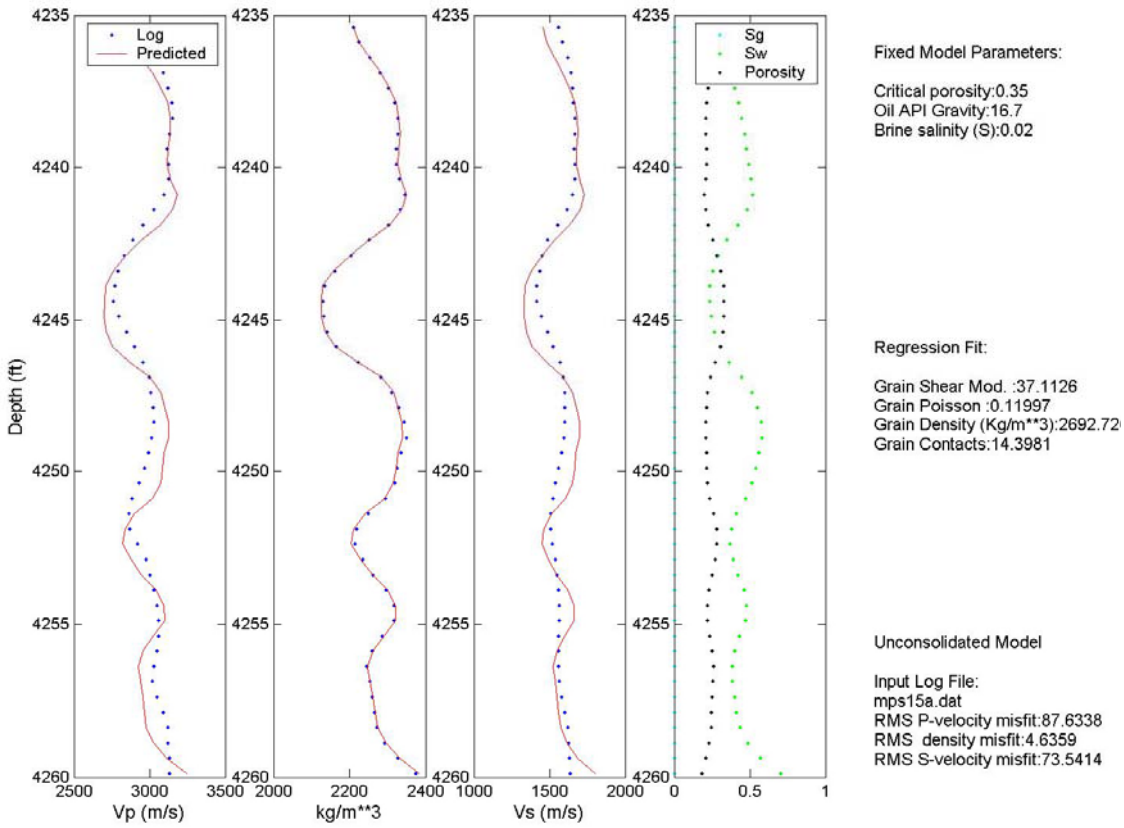

Figure 4. Rock properties model based on un-consolidated sandstone model (Dvorkin & Nur, 1996). Measured log values shown as blue dots. Parameters (right side) are derived from a simplex minimization of the misfit between observed and calculated V_p, V_s and density logs. Predicted V_p, V_s and density are shown as red lines.

A critical porosity appropriate for sandstone of 35% is assumed. Oil API gravity and brine salinity are taken from measured values. The regression determined values of the grain shear modulus and Poisson ratio are appropriate for quartz grains. The model parameters are determined for the reservoir interval in the logs. The full geophysical models are built by interpolating available well logs in 3D using the seismic reservoir surfaces as a spatial guide. This produces a background model in V_p, V_s, density and resistivity. The reservoir flow simulations, which only cover the reservoir interval, are then filled in at the time intervals where flow simulations were done. The model shown in Figure 4, along with Archie's law, is used to convert the porosity, water saturation, oil saturation, gas saturation, CO_2 saturation, pressure and temperature from the flow simulation to V_p, V_s, density and electrical resistivity.

Gravity modeling

A snapshot of the model at initial conditions, before CO_2 injection begins, is shown in Figure 5. Figure 5a is a cross-section of bulk density as a function of depth and horizontal distance between a pair of injection wells. In this figure, gravimeters are located in two wells roughly 8 km apart. The reservoir interval is outlined in white on Figure 5a. Figure 5b is a plan view of the density at initial conditions at a depth of 1,200 m with positions of 23 injecting wells taken from the reservoir simulation. The positions of the gravimeters are indicated by black squares. Spacing between the gravimeters in depth (z) is 10 m outside of the reservoir and 5 m inside of the reservoir. The white circle in the upper part of Figure 5b indicates a well for which borehole gravity responses are shown in Figure 11 and 12.

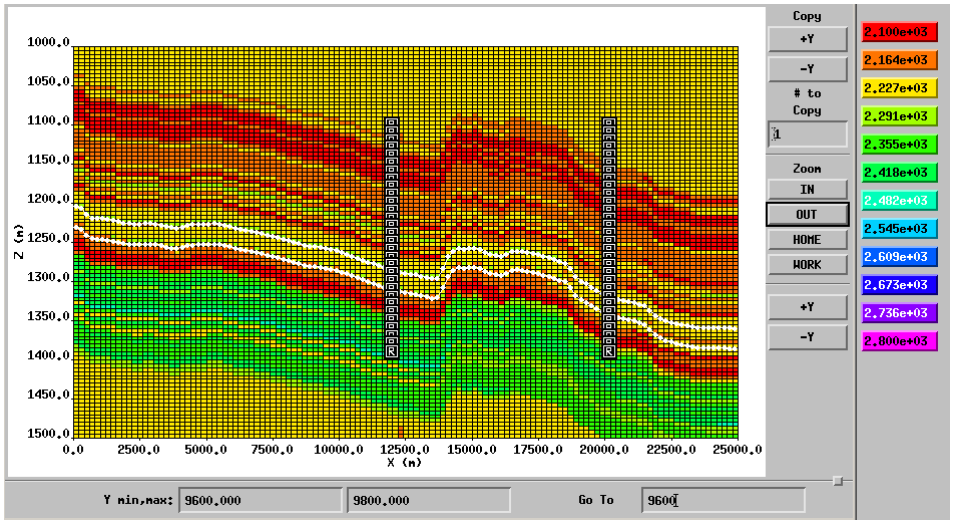

Figure 5a. Cross-section of a density field (kg/m^3) as a function of depth and horizontal position.

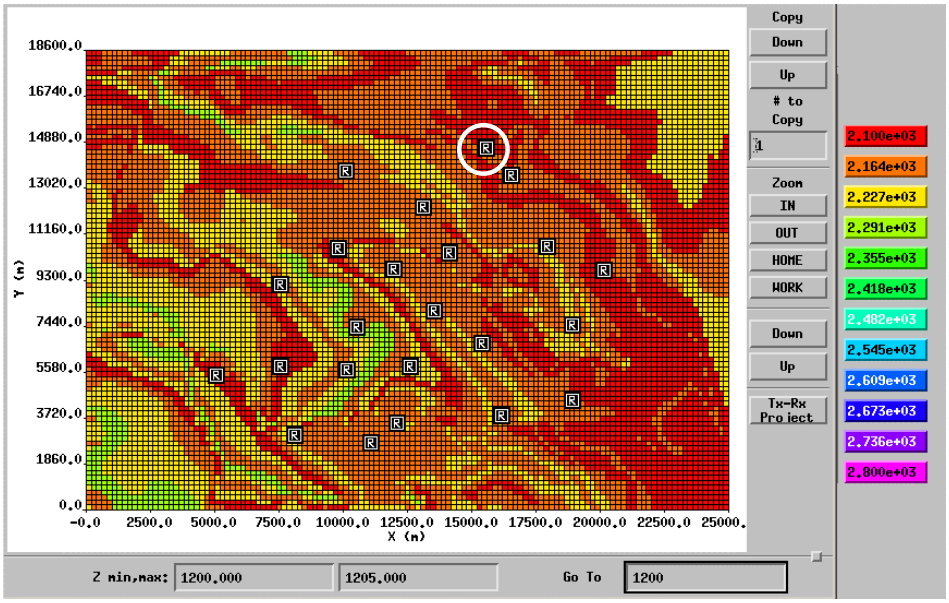

Figure 5b. Plan view of a density (kg/m^3) field at a depth z = 1,200 m. The white circle indicates the well location used for borehole gravity calculations shown in Figures 11 and 12.

The surface gravity response was calculated on a grid of stations with 1 km spacing from 2,000 m to 22,000 m in x and from 2,000 m to 16,000 m in the y direction. In general since CO_2 is less dense (at reservoir conditions) than either oil or water, addition of CO_2 to the reservoir will cause a reduction in the measured gravitational attraction either at the surface or in a borehole.

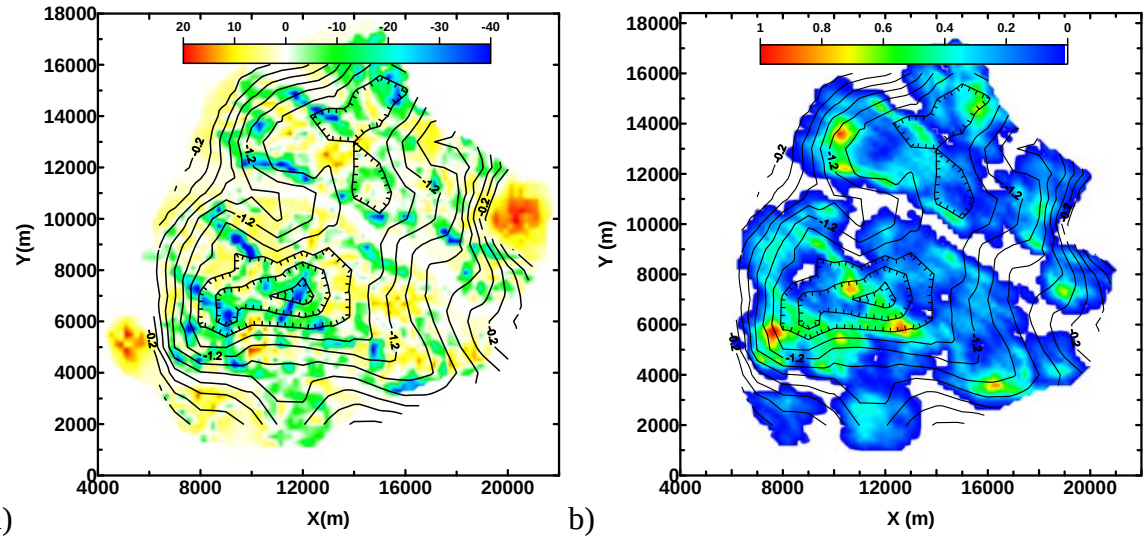

a) b)

Figure 6. (a) Plan view of the net change in density (kg/m^3) within the reservoir. (b) Plan view of the net changes in CO_2 saturation within the reservoir. The change in G_z at the surface for the same time period is shown as black contours with hatch marks indicating decreasing G_z values.

The change in the vertical attraction of gravity (G_z) at the ground surface between 2020 and initial conditions is overlaid as black contours in Figure 6a on the net density changes within the reservoir. The peak-to-peak change in G_z is on the order of 2 μgal, which would be in the noise level of a field survey using current technology (Hare, 1999). The changes in the vertical gradient of gravity (dG_z/dz) between 20 years into CO_2 injection and initial conditions (not shown) are approximately 0.01 Eötvos units (EU), and also below the noise level of current instruments. The high spatial variations of the net density changes within the reservoir are expressed as a filtered response at the surface and only show the average changes on a larger scale. It should be noted that petroleum reservoirs in general, and this reservoir in particular, are thinner (30 m) than most brine formations considered for CO_2 sequestration (100–200 m). This difference means that while the calculated response for Schrader Bluff at the surface are below current technology repeatability, brine formations at the same depths would produce measurable responses. This is the experience at the Sleipner CO_2 project (Nooner et al., 2003) for a gravity survey conducted in 2002 and not yet published. These results suggest future analysis to determine the maximum sensitivity of G_z and dG_z/dz that could be obtained by permanent emplacement of sensors with continuous monitoring coupled with surface deformation measurements to reduce noise levels.

Figure 6b shows the change in surface gravity G_z as black contours overlaid on the net change in CO_2 saturation within the reservoir. Because the density changes within the reservoir are caused by a combination of CO_2, water and oil saturation changes as the WAG injection proceeds, there is not a one-to-one correlation in space between either the net change in density and the change in G_z or the net change in CO_2 saturation (S_{CO2}) and the change in G_z. There is correlation between the change in surface G_z and the net change in S_{CO2} on a large scale. For example, the largest changes in S_{CO2} occur in the

south-west quadrant of the image (Figure 6b) where the largest change in G_z occurs. This scenario, injecting CO_2 into an oil reservoir with multiple fluid components, is a worst case for the use of gravity to directly map changes in S_{CO2}. In a CO_2 injection into a brine formation there would only be water and CO_2, in this case the net changes in density within the reservoir would directly correlate with the net changes in S_{CO2} as would the change in G_z at the surface.

Access to boreholes allows the gravity measurement to be made closer to the reservoir, thus strengthening the signal compared to observations made on the surface. Figure 7a shows the change in G_z (2020 – initial) at a depth of 1,200 m (just above the reservoir in this section of the field), while Figure 7b is a change in dG_z/dz at the same depth. In both figures, the data are calculated on the same grid of 1km by 1km site locations as on the surface. The color images in Figures 7a and 7b are the net density changes in the reservoir from Figure 7a. The changes in G_z and dG_z/dz respectively, correlate directly with the maximum density changes. The magnitude of the changes in both G_z and dG_z/dz is larger than for surface measurements, although only the change in G_z would be measurable in the boreholes with current commercial technology. It should be noted however that work on more sensitive borehole G_z and dG_z/dz meters is ongoing and has the potential to significantly lower the sensitivity of such devices in the near future (Thomsen et al, 2003).

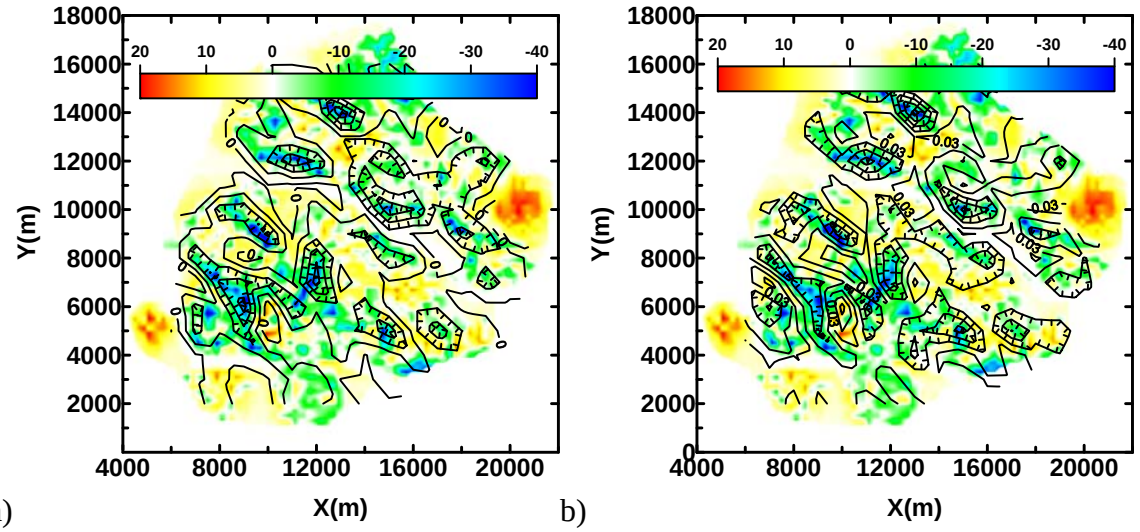

a) b)

Figure 7. (a) Plan view of the color coded net change in density within the reservoir (2020-initial). The change in G_z (μGal) at a depth of 1,200 m is overlaid as black contours. The peak-to-peak change in G_z is approximately 10 μGal. (b) The change in dG_z/dz (EU) at a depth of 1,200 m overlaid on the net change in density. The peak-to-peak change in dG_z/dz is approximately 0.25 EU.

While Figure 7 illustrated the potential resolution by measuring close to the reservoir, access though the existing injection wells would substantially reduce the data coverage. Figure 8a shows a map of contoured changes in G_z measured only in the 23 boreholes at a depth of 1,200 m. Figure 8b is a net change of CO_2 saturation for comparison. Figure 8a was generated using a minimum curvature algorithm for data interpolation; however it is representative of the general features present in all of the other types of interpolation tested. In general, interpretation of the interpolated G_z changes from the boreholes would lead to an over estimate of the CO_2 saturation changes in the reservoir. This problem is particularly evident at the north end of the field where increased CO_2 saturation at two isolated wells produces an interpolated image that would be interpreted as increased CO_2 between the wells where none exists.

Borehole measurements would have to be used in conjunction with some form of surface measurement to guide the interpolation between wells. Alternatively, pressure testing between wells could provide estimates of spatial variations in permeability that could be used to condition, in a statistical sense, interpolation of the borehole gravity data. Many possibilities exist for combining the borehole data with other information in order to produce more accurate maps of change within the reservoir. This is an area where further work could be done.

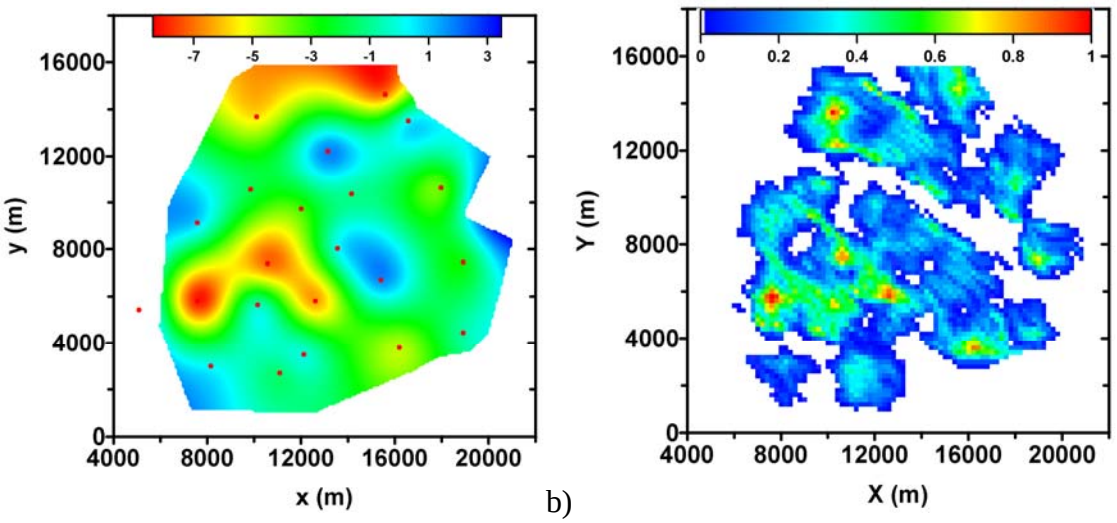

a) b)

Figure 8: (a) Plan view of the change in G_z (μGal) at a depth of 1,200 m between 20 years into CO_2 injection and initial conditions using 23 wells indicated by red dots. (b) Plan view of the net change in S_{CO2} within the reservoir between 20 years into CO_2 injection and initial condition.

In addition to considering spatial variations in G_z and dG_z/dz on both the surface and at a constant depth within boreholes the response of G_z and dG_z/dz in vertical profiles down boreholes has been considered. Figure 9 is the change in S_w between 2020 and initial conditions along a vertical slice through the reservoir at an injection well indicated by a white circle in Figure 5b. Figure 10 shows the change in S_{CO2} between 2020 and initial conditions. At the top of the reservoir near the injection well, S_w decreases while S_{CO2} increases. At the bottom of the reservoir, both S_{CO2} and S_w increase slightly. G_z measured in the borehole, shown in Figure 11a, reflects this change by a decrease in the response at the top of the reservoir, and an increase in the response at the bottom. The change in G_z is ± 8 μGal. The reservoir interval is between 1,325 and 1,350 m at this location. The change in G_z between 2020 and initial conditions (Figure 11b) clearly identifies the position of the reservoir. The sign of the change reflects the changes in the local densities caused by the combined changes in all fluids (oil, water and CO_2). The reservoir is outlined by the shaded blue area.

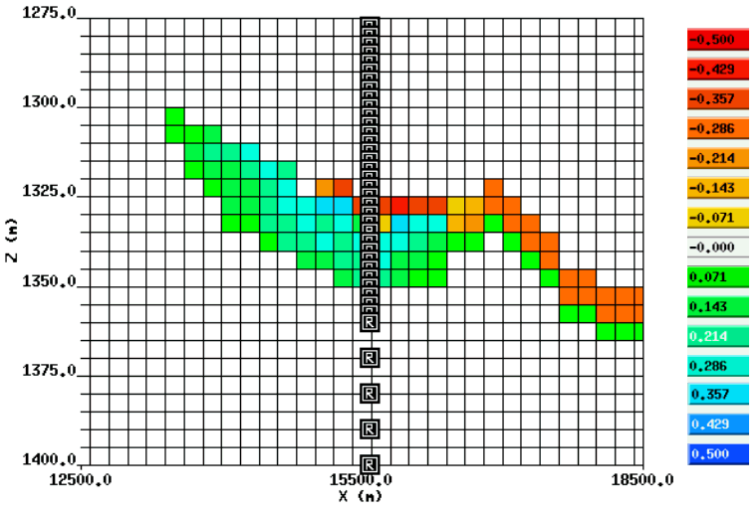

Figure 9. Change in S_w between 2020 and initial conditions. Greens and blues are an increase in S_w, yellows and reds are a decrease.

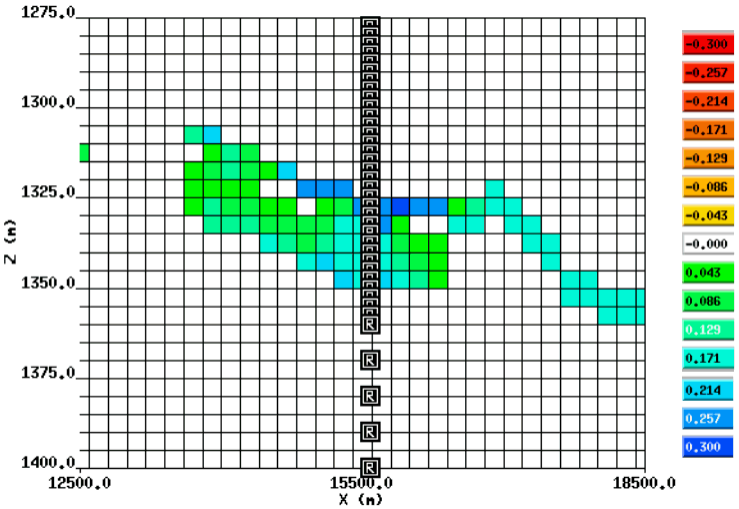

Figure 10. Change in S_{CO2} between 2020 and initial conditions. Greens and blues are an increase in S_{CO2}, yellows and reds are a decrease.

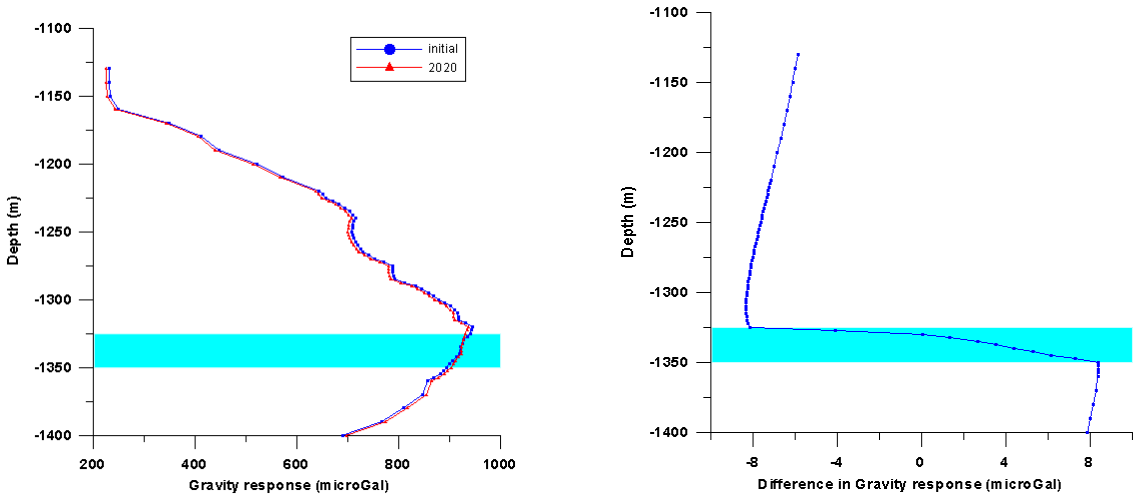

(a) (b)

Figure 11. (a) Borehole G_z for initial conditions (dark blue line) and 2020 (red line), (b) Change in G_z between 2020 and initial conditions. The reservoir interval is indicated by the light blue area.

The vertical gradient response (dG_z/dz) is shown in Figure 12a, and the change between 2020 and initial conditions is shown in Figure 12b. The change in the response is about 0.1 EU, which is not measurable with current technology.

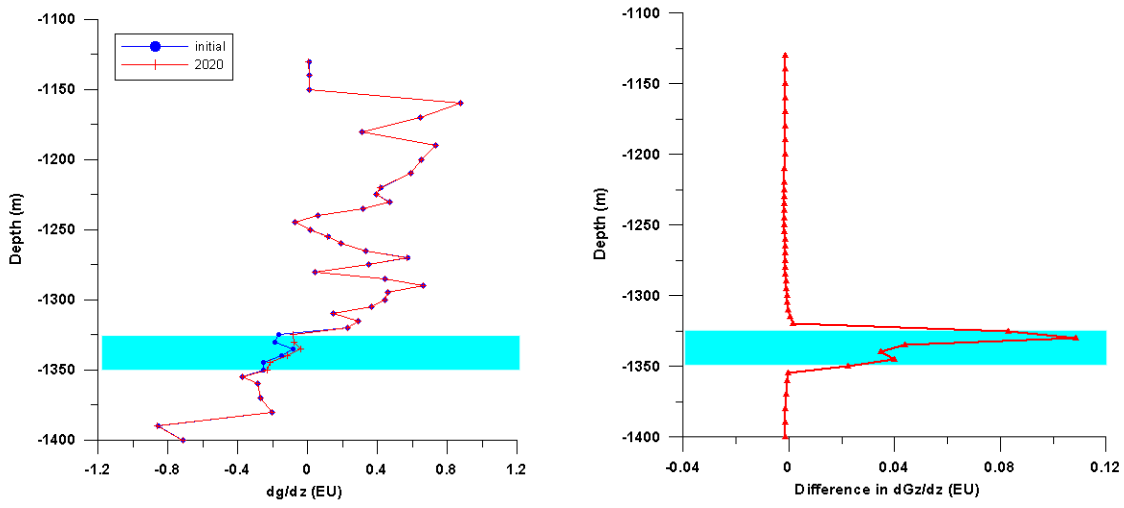

(a) (b)

Figure 12. (a) Borehole vertical gradient response (dG_z/dz) for initial conditions (dark blue line) and 2020 (red line), (b) Change in dG_z/dz between 2020 and initial conditions. The reservoir interval is indicated by the light blue area.

Popta et al. (1990) showed that a geological structure with a sufficient density contrast can be detected by borehole gravity measurements if the observation well is not further away than one or two times the thickness of the zone of density contrast. Figure 13 shows a CO_2 wedge of 250 m radius and density of 2,260 kg/m^3 (representing 20% CO_2 saturation in 20% porosity) inside of 100 m thick sand layer with a density of 2,285 kg/m^3 at the depth of 1 km. The background density is 2,160 kg/m^3. The borehole gravity response as a function of distance from the right edge of the wedge is shown in Figure 14a. The maximum response at the edge of the CO_2 wedge is 10 μGal (due to 1% change in density). The responses decrease with distance away from the wedge. 50 m away from the wedge the response is 6 μGal, 100 m away response decreases to 4.4 μGal, and 200 m away it is down to 2.5 μGal. The borehole vertical gradient response for the same model is shown in Figure 14b. The response changes from 7 EU at the edge of the CO_2 wedge to 1 EU 50 m away from the edge.

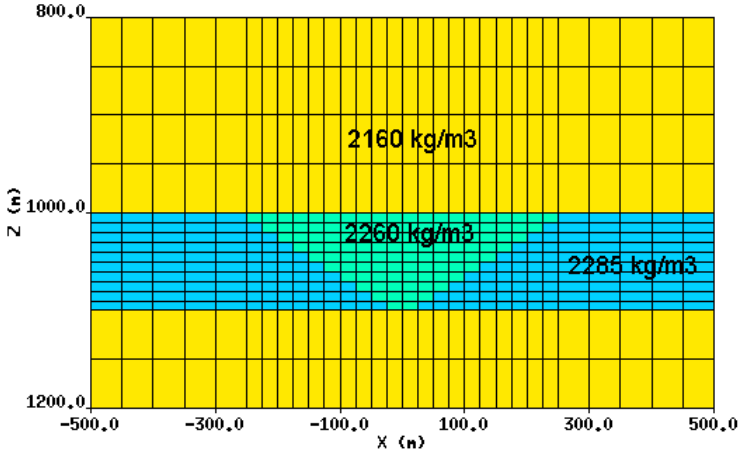

Figure 13: CO_2 wedge model.

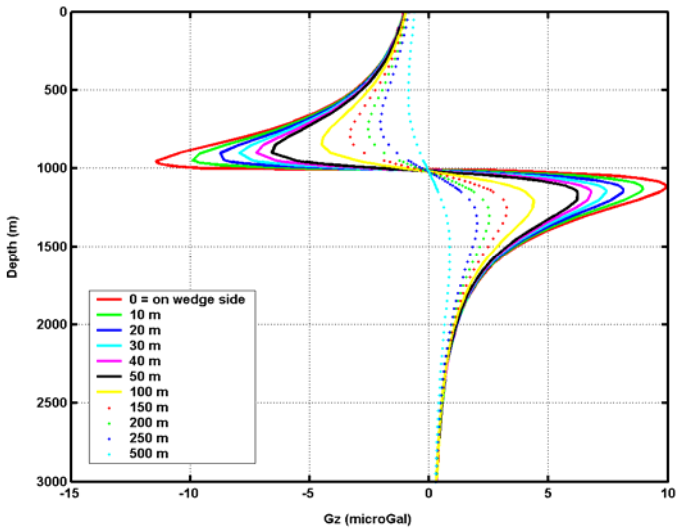

Figure 14a: Borehole gravity response of the model in Figure 13 as a function of distance from the wedge edge.

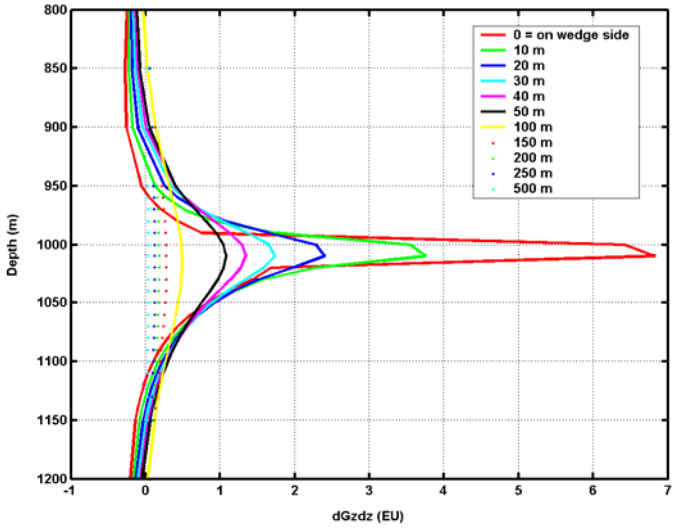

Figure 14b: Borehole vertical gradient gravity response of the model in Figure 13 as a function of distance from the wedge edge.

Current borehole gravimeter technology has a repeatability of around 5 μGal for G_z, this means that with current technology borehole measurements are sensitive to changes in a zone up at distances equal to the zone thickness away from the zone edge.

Seismic modeling

The flow simulation models for Schrader Bluff have been converted to acoustic velocity, shear velocity and density. A simulated seismic line has been calculated running approximately N45°E across the reservoir. The elastic response to a 50 Hz Ricker wavelet was calculated. The general increase in S_{CO2} in portions of the reservoir near injection wells produces an approximately 20% decrease in seismic velocity as shown in Figure 15 (change in P-wave velocity between 2020 and 2005). The S_{CO2} and S_w changes are shown in Figures 16 and 17 respectively. The seismic pressure responses, for a single shot located at 7,500 m (covering the area of the reservoir with maximum change in S_{CO2}) on the 2D profile, for 2005 and 2020 are shown in Figure 18 with the difference shown in Figure 19. There is a significant class 3 type AVO effect as S_{CO2} increases in the reservoir.

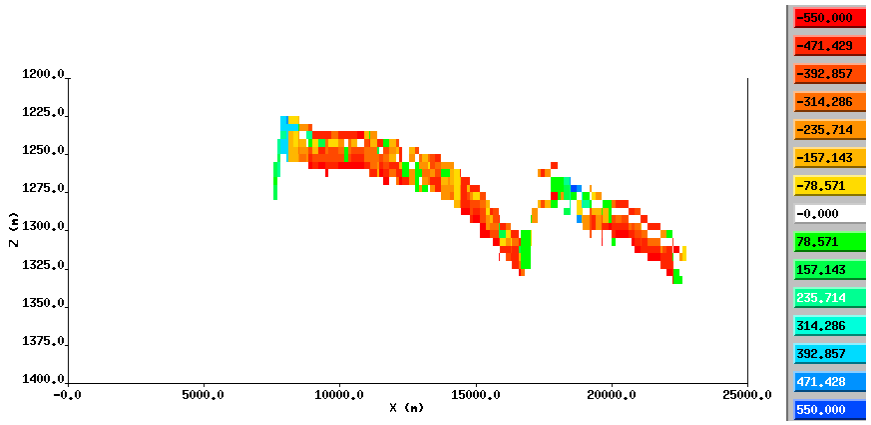

Figure 15. Change in the acoustic velocity (Vp) between 2020 and 2005 along a 2D profile extracted form the 3D model volume. The profile runs N45°E across the 3D model. Note the significant decrease in acoustic velocity associated with the increase in S_{CO2} (Figure 16).

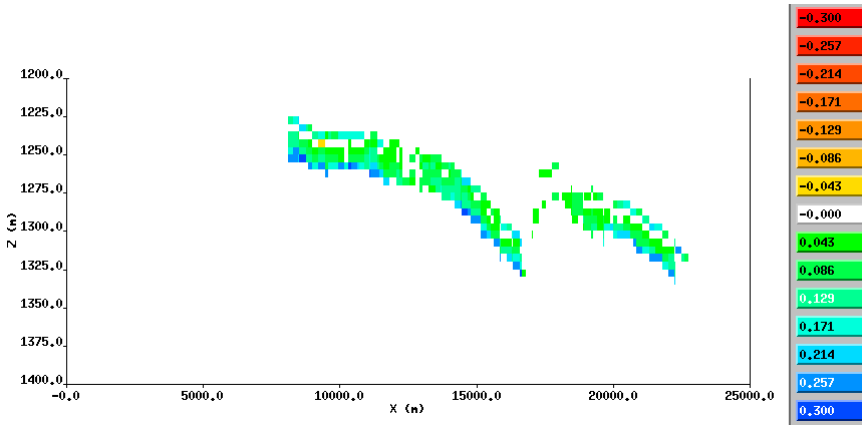

Figure 16. Change in the S_{CO2} between 2020 and 2005.

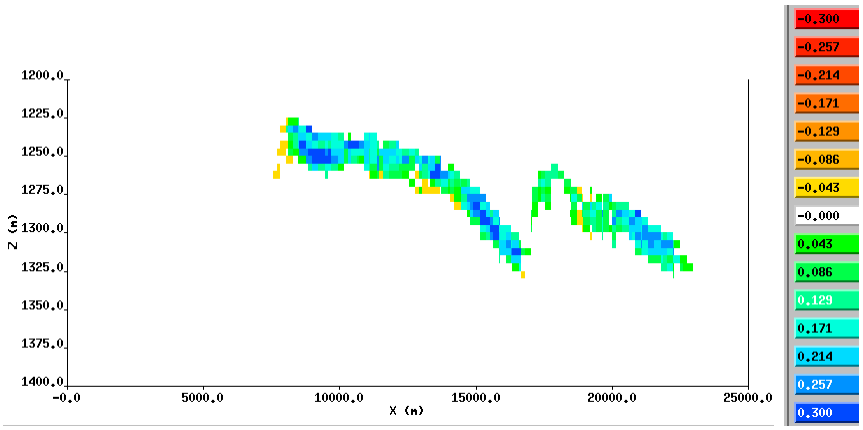

Figure 17. Change in S_w between 2020 and 2005.

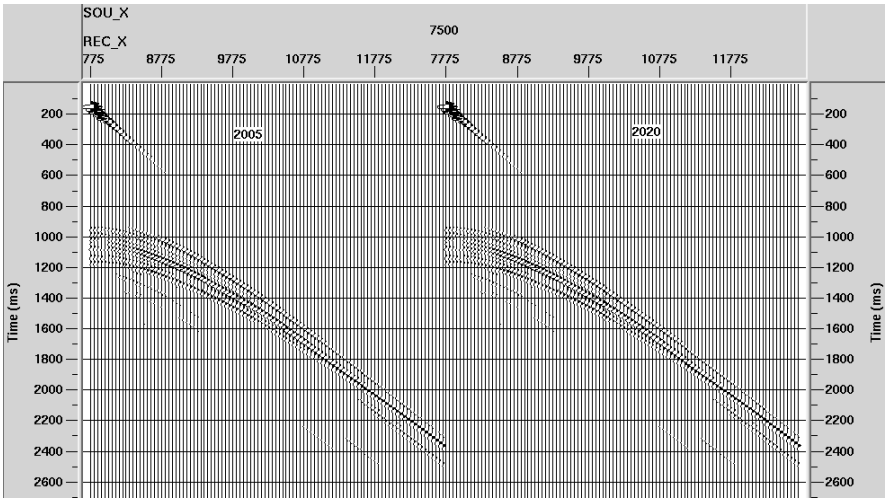

Figure 18. Seismic pressure response (shot gather) for 2005 and 2020.

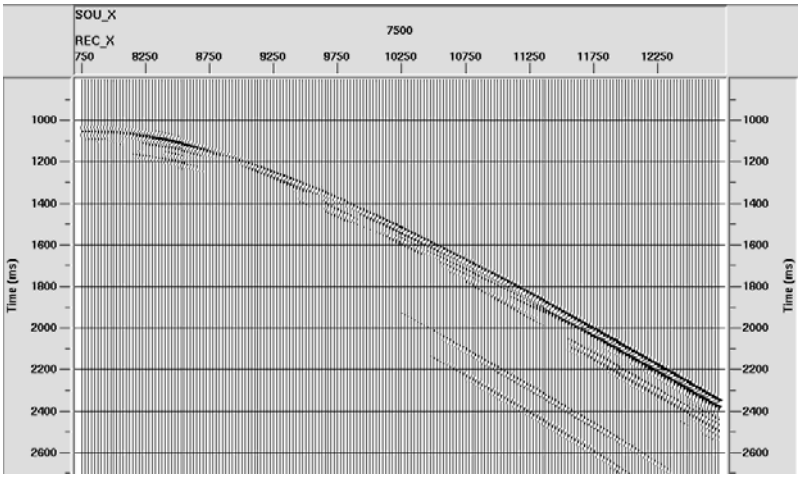

Figure 19. Change in pressure response (shot gather) between 2020 and 2005. Note amplitude change and AVO effects associated with S_w and S_{CO2} changes in the reservoir.

The pressure response was sorted to CDP gathers, NMO corrected and stacked to produce the sections for 2005 and 2020 shown in Figure 20. The red line is a constant time horizon within the reservoir for reference. The 30 m reservoir interval is not uniform and is comprised of 5 m thick substrata, each of which has reflection coefficients at their top and base that vary with S_{CO2}. These sub-strata are all below the seismic tuning thickness. This produces a seismic response without a clear top and base reflector. There is a significant increase in S_{CO2} to the right of CDP 8412.5 producing the large change in the stacked sections shown in Figure 20.

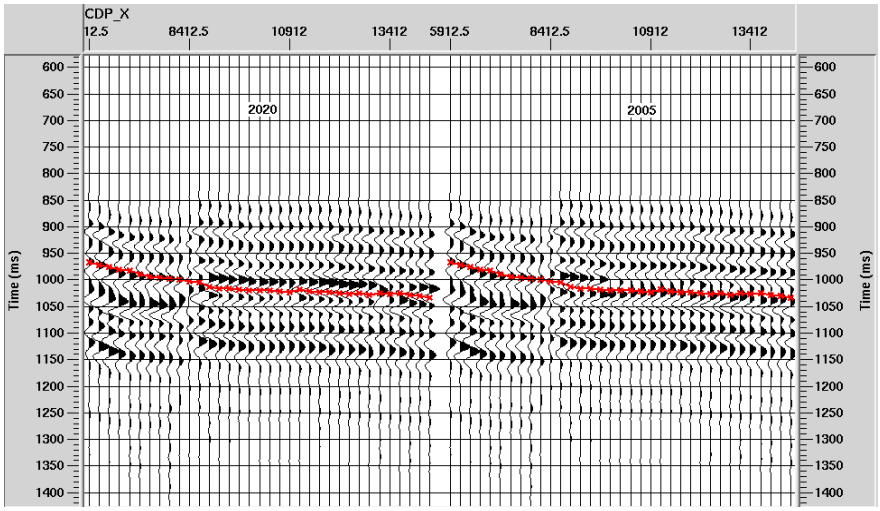

Figure 20. Stacked section for 2005 and 2020.

The change in the stacked sections between 2020 and 2005 is shown in Figure 21. Below the areas of major change in the reservoir (to the right of CDP 8412.5) the decrease in the velocity of the reservoir produces a time shift in the 2020 seismic responses below the reservoir, resulting in the events around 1,100 ms that do not reflect CO_2 saturation changes at this depth, only the time shift from CO_2 above.

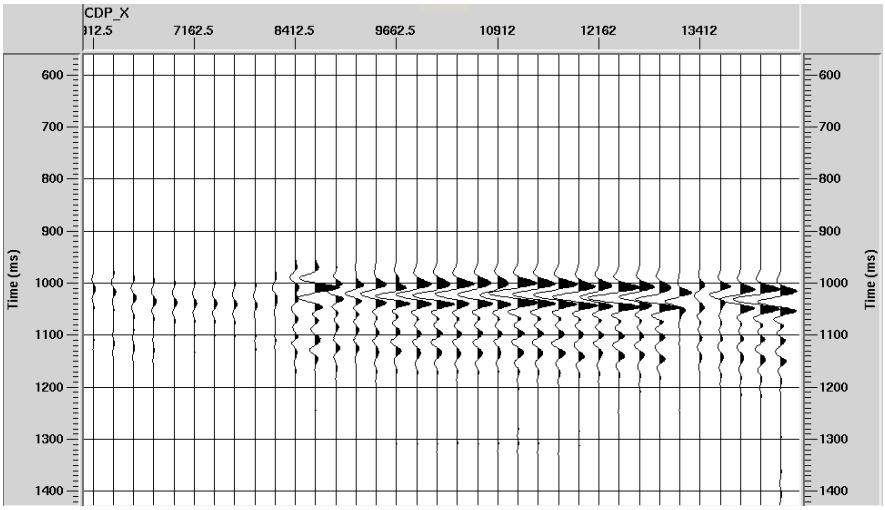

Figure 21. Change in the stacked sections between 2020 and 2005 (2020-2005).

There is a large, and easily measurable, change in the stacked trace amplitude associated with the reservoir caused by the changes in S_w and S_{CO2}. In addition, there is a change in the AVO effects as seen in Figure 19. Both amplitude and AVO can be exploited to make quantitative estimates of saturation changes under certain conditions. Forward calculations using the Zoeppritz equation for both the 2005 and 2020 models provide insight into the AVO dependence on model parameters. The forward modeling creates a synthetic seismic gather from a given set of elastic parameters V_P, V_S and density as a function of depth. The full Zoeppritz equation is used to compute the acoustic to acoustic (pp) reflection coefficient Rpp(θ) for each angle and at each layer boundary. Synthetic seismic CDP gathers are calculated by convolving the angle dependent reflection coefficients with a 50 Hz Ricker wavelet. The convolution model assumes plane-wave propagation across the boundaries of horizontally homogeneous layers, and takes no account of the effects of

geometrical divergence, inelastic absorption, wavelet dispersion, transmission losses, mode conversions and multiple reflections.

The change in V_P, V_S, and density within the reservoir (between 1250 and 1275 m) is shown in Figure 22.

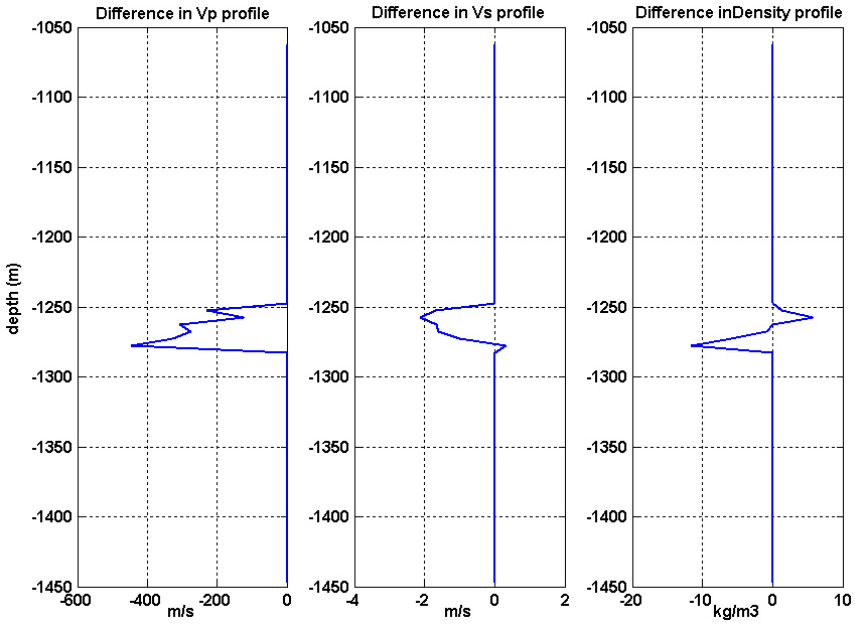

Figure 22. Difference in V_P, V_S, and density profiles between 2020 and 2005 for the Schrader Bluff model at the center of maximum CO_2 saturation increase.

The synthetic CDP gathers as a function of angle are shown in Figures 23a and 23b for 2005 and 2020 respectively. The change in reflection amplitude between 2020 and initial conditions is shown in Figure 24. The AVO response of the composite reflections from the reservoir interval shows increasing negative amplitude with offset, a typical Class 3 gas response. The negative trough (associated with the top of the reservoir) increases its magnitude with offset and is followed by an increasing peak amplitude with offset

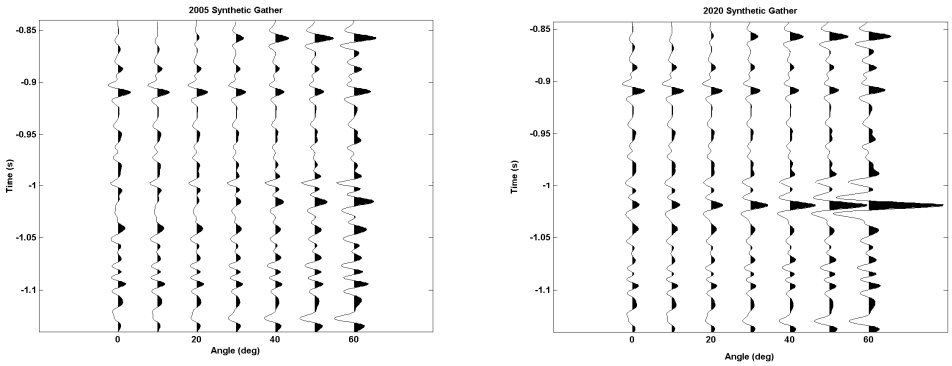

(a) (b)

Figure 23. Synthetic gather for (a) 2005 and (b) 2020.

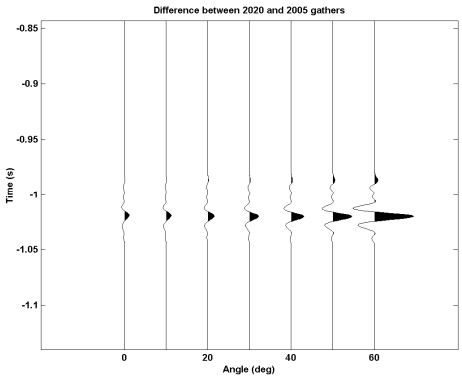

Figure 24. Difference between 2020 and 2005 gathers.

Use of AVO in fluid saturation prediction

The AVO attributes of reflections from the reservoir can be used to estimate fluid saturations under certain circumstances. AVO data can be used to estimate the acoustic and shear impedance of the reservoir (Castagna et al., 1998). When used in a time-lapse sense, these data can provide estimates of the change in water saturation and pressure within the reservoir (Landro, 2001). The ability to predict changes in water saturation and pressure within a reservoir is illustrated in Figure 25. In Figure 25 the rock properties model derived for the North Sea sands of the Troll reservoir (Dvorkin and Nur, 1996) is used to calculate the changes in shear and acoustic impedance of the reservoir as the water saturation and pore pressure for two cases of oil saturation as CO_2 is introduced. The first

case (open circles) has initial oil and water saturation of 50%, as CO_2 is introduced it replaces water. The second case has an initial oil saturation of 60% and 40% water, with CO_2 replacing water. In both cases S_{CO2} ranges from 0 to 30%. Each point in the figure represents a unique value of S_W and S_{CO2} with the oil saturation held fixed at either 50% or 60%. S_{CO2} values increase in increments of 0.015% from right to left on the figure, and pore pressure increases and decreases (indicated by arrows) from the reference pressure of 24.24 MPa by increments of 0.7 MPa.

Figure 25 illustrates three important points; 1) if the oil saturation is known the changes in shear and acoustic impedance of the reservoir can determine the change in pressure and CO_2 saturation, 2) the changes in the shear impedance required to make the estimates is quite small and would require extremely good shear data, 3) an uncertainty in the oil saturation level of 10% in this example has only a small effect on the estimated values of changes in S_{CO2} and almost no effect on the estimates of pressure change.

An uncertainty on the value of oil saturation has limited effects in these calculations because of the relative similarity of the bulk modulus and density of oil compared to water when either is compared to the properties of CO_2. The situation is significantly different if there is hydrocarbon gas (such as methane) in the reservoir. In this case (due to the extreme differences between the properties of methane and water) even a small uncertainty in the hydrocarbon gas saturation leads to very large uncertainties in the estimated values of pressure and CO_2 saturation changes, making this technique essentially unusable unless an independent estimate of water saturation or gas saturation can be obtained from other methods (Hoversten et al., 2003).

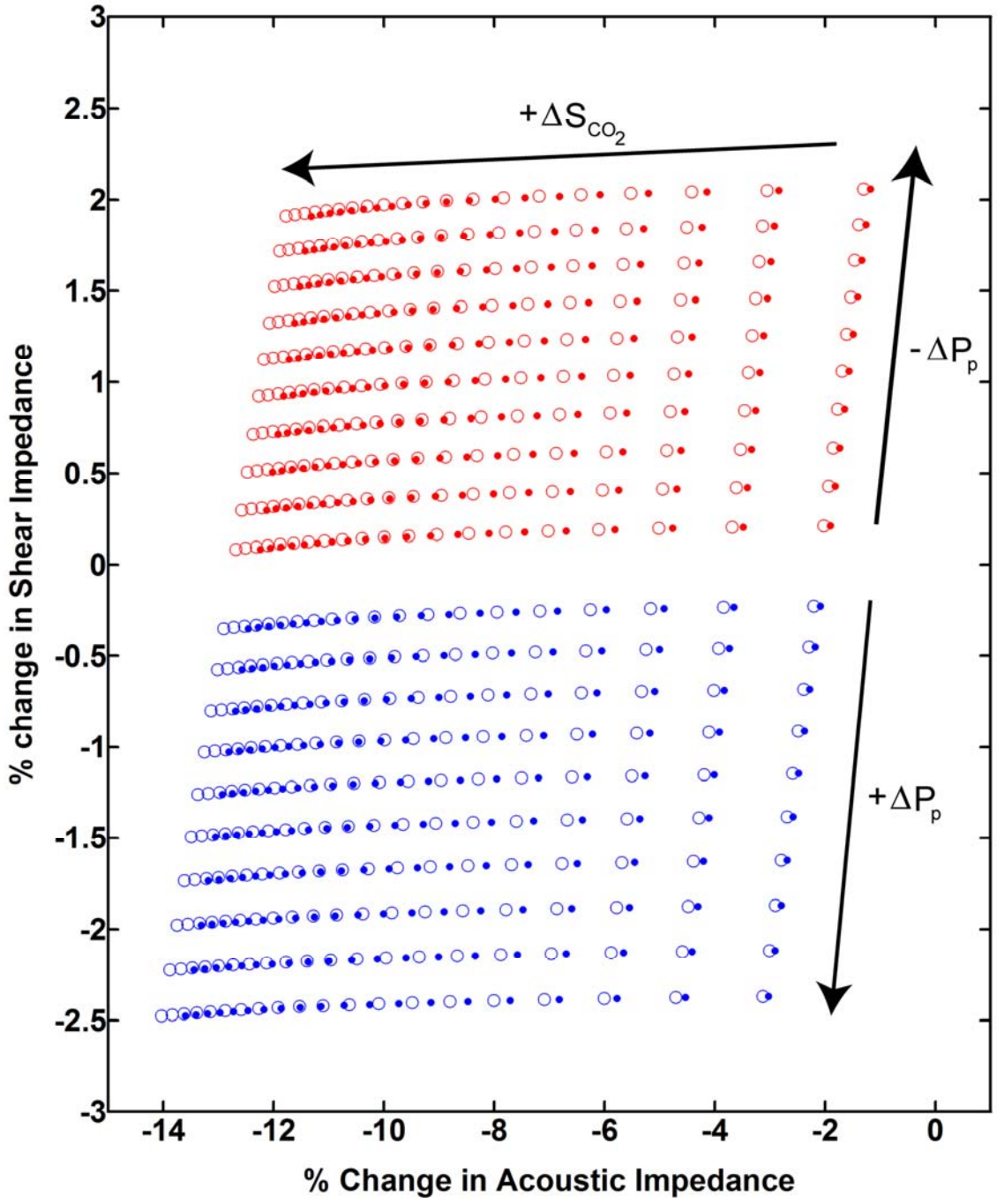

Figure 25. Each point represents a unique value of changes in pore pressure (ΔP_p) and CO_2 saturation (ΔS_{CO2}) as a function of changes in the shear and acoustic impedance of the reservoir. Open circles represent oil saturation of 50% with CO_2 replacing water. Filled dots represent oil saturation of 60% with CO_2 replacing water. Initial pore pressure is 25.24 MPa, initial S_{CO2} is 0%. S_{CO2} increments are 0.015 and pressure increments are 0.7 MPa.

While estimation of changes in fluid saturation using AVO is complicated by the multiple fluid components in oil or gas reservoir, the situation is simpler in a brine reservoir. For cases were CO_2 is injected into a brine reservoir there are only two fluid components (brine and CO_2) and the added constraint that their saturations levels sum to one. In this case AVO information can more easily be used to estimate the level of CO_2 in the reservoir. The following example illustrates this process. An unconsolidated North Sea sand of the Troll reservoir (Dvorkin and Nur, 1996) that is encased in shale is assumed to contain 50% brine and 50% CO_2 as the reference point for these calculations. Pressure and temperature are such that the CO_2 is in the liquid state. The values of CO_2 (and hence water) saturation and pore pressure are varied about this starting point and the acoustic and shear velocities as well as density are calculated.

The reflection coefficient at the top of the reservoir can be approximated (Shuey, 1985) by:

$$R(\theta) \approx A + B\sin^2(\theta) + C\sin^2(\theta)\tan^2(\theta) \tag{2}$$

where θ is the average of the reflection and transmission angle for a plane wave hitting the interface. The constants A and B are referred to as the intercept and slope respectively in the AVO literature. The constants A, B and C are functions of the velocity and density of the media on either side of the reflecting interface and are given by:

$$A = 1/2(\Delta V_p / \langle V_p \rangle + \Delta\rho / \langle \rho \rangle \tag{3}$$

$$B = 1/2(\Delta V_p / \langle V_p \rangle - 2(\langle V_s \rangle / \langle V_p \rangle)^2 (2\Delta V_s / \langle V_s \rangle + \Delta\rho / \langle \rho \rangle)) \tag{4}$$

$$C = 1/2(\Delta V_p / \langle V_p \rangle \tag{5}$$

where ΔV_p is the change in acoustic velocity across the interface and $\langle V_p \rangle$ is the average acoustic velocity across the interface, ΔV_s , $\langle V_s \rangle$, $\Delta\rho$, and $\langle \rho \rangle$ are changes and averages for shear velocity and density respectively. If time lapse seismic data is acquired, and A and B are estimated from the AVO data and used to calculate ΔA and ΔB, the associated

ΔS_{CO2} and ΔP_p can be estimated from model based calculations such as are illustrated in Figure 26.

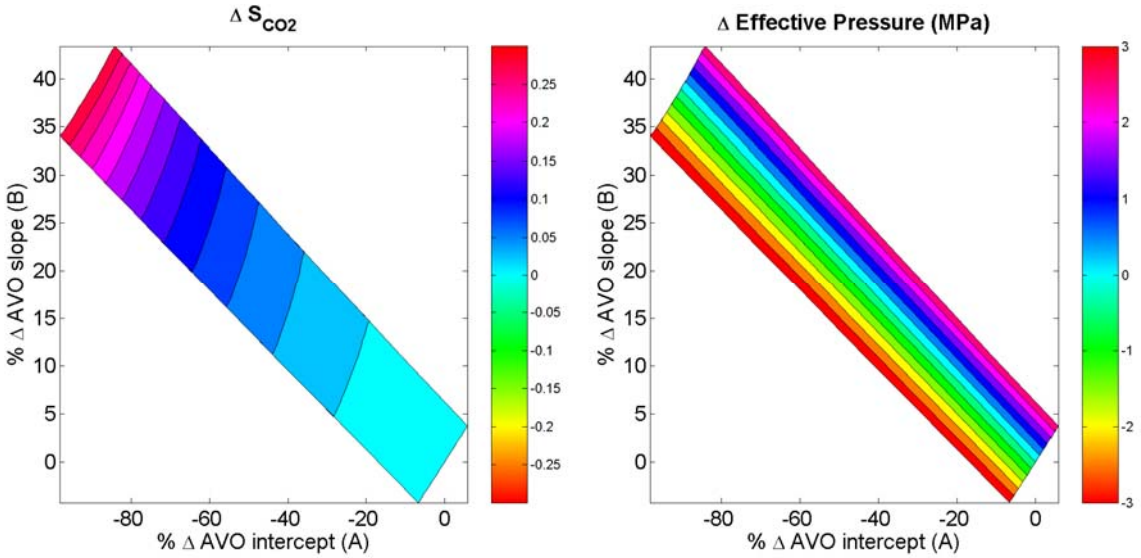

Figure 26. Contours of the change in CO_2 saturation (left panel) and effective pressure (lithostatic – pore pressure) (right panel) as function of the change in the AVO intercept (A) and slope (B) for an unconsolidated sand surrounded by shale.

This example illustrates a theoretical case without noise in the seismic data, in practice estimation of the "slope", B, is the most difficult. Extremely high signal to noise (S/N) seismic data would be required for accurate estimates of B and hence accurate estimates of pressure and saturation changes.

Electromagnetic modeling

The electrical resistivity of reservoir rocks is highly sensitive to changes in water saturation. This can be seen from Archie's Law (Archie 1942), which has been demonstrated to accurately describe the electrical resistivity of sedimentary rocks as a function of water saturation, porosity, and pore fluid resistivity. Figure 27 shows the rock bulk resistivity (Ωm) as a function of gas saturation (1–water saturation) for a reservoir with brine resistivity equivalent to sea water (ρ_{brine} = 0.33) with 25% porosity.

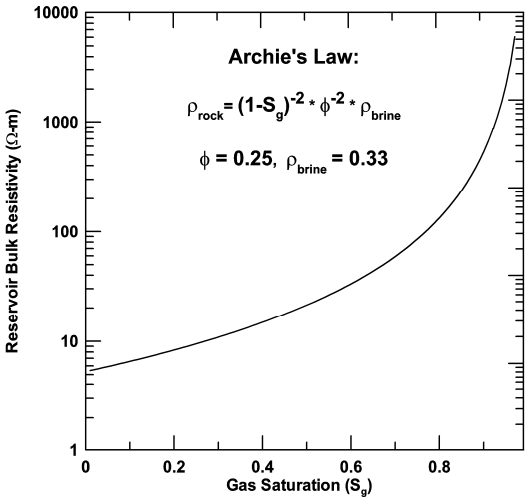

Figure 27. Reservoir bulk resistivity as a function of gas saturation (S_g). Porosity = 25%.

All petroleum fluids (oil, condensate, and hydrocarbon gas) as well as CO_2 are electrically resistive, hence the relation shown in Figure 27 is appropriate for any combination of oil, hydrocarbon gas, condensate or CO_2.

The bulk resistivity in Figure 27 is plotted on a log scale to span the large range of resistivity values as a function of the gas saturation (S_g). This high sensitivity to water saturation in a reservoir can be exploited by electromagnetic (EM) techniques where the response is a function of the earths electrical resistivity. Of all the possible combination of EM sources and measured EM fields one system combines both relative ease of deployment with high sensitivity to reservoirs of petroleum scale and depth. This technique uses a grounded electric dipole that is energized with an alternating current at a given frequency to produce time varying electric and magnetic fields that can be measured on the earth's surface. The electric dipole can consist of two steel electrodes (1 m^2 plates or sections of drill pipe) buried at a shallow depth (1-10 m) separated by 100 m and connected by cable to a low power generator (a portable 5,000 W generator is sufficient).

The measured data would consist of the electric field at a given separation from the transmitter acquired on the surface or within the near surface.

To simulate such an EM system we have calculated the electric field on the surface of the Schrader Bluff model using 100 m electric dipoles operating at 1 Hz an measuring the resulting electric field at a separation of 2 km in-line with the transmitting dipole. Figure 28 shows the amplitude of the generated EM field at 2 km separation and 1 Hz together with the natural background electric field generated from worldwide thunderstorms and pulsations in the earths ionosphere (the source field for the magnetotelluric method). The significance of Figure 28 is that the generated electric field for the Schrader Bluff model, using only a small portable generator (producing a 10 A current in the source dipole) is an order of magnitude above the background electric field (noise) at the operating frequency of 1 Hz. This means that synchronous detection of the signal combined with stacking can recover signal variations to better than 1 percent.

Figure 29 shows the net change in water saturation within the reservoir (vertically integrated ΔS_w) between 2020 and initial conditions. The change in the electric field amplitude for the same interval is overlaid as black contour lines, with peak-to-peak amplitude of 1.2%. There is a direct one-to-one correspondence with the change in S_w and the change in the electric field amplitude. While this signal level is low, it can be measured give the signal-to-noise ratio of the data (Figure 28). While this represents a potential low-cost monitoring technique it is best suited for CO_2 – brine systems where there is a one-to-one correlation between the change in water saturation and the change in CO_2 saturation (since $S_w + S_{CO2} = 1$). In petroleum reservoir such as Schrader Bluff the presence of hydrocarbon as additional fluids eliminates the one-to-one correlation between changes in S_w and changes in S_{CO2}. This is illustrated in Figure 30 where the same changes in electric field amplitude are overlaid on the net change in the CO_2 saturation within the reservoir between 2020 and initial conditions. In this case we see that the correlation between changes in S_{CO2} and changes in the electric field amplitude are not as good as seen between changes in S_w and the electric field data.

This type of EM technique has not yet been employed as a monitoring tool within the petroleum industry. However, EM technology is currently the subject of a significant upsurge in industry interest. Several commercial contractors are now offering this technique as a survey tool, most notably, in the offshore environment where it is currently being used as an exploration tools (Ellingsrud et al. 2002). The equipment and service providers exist to apply this technique for monitoring in the future.

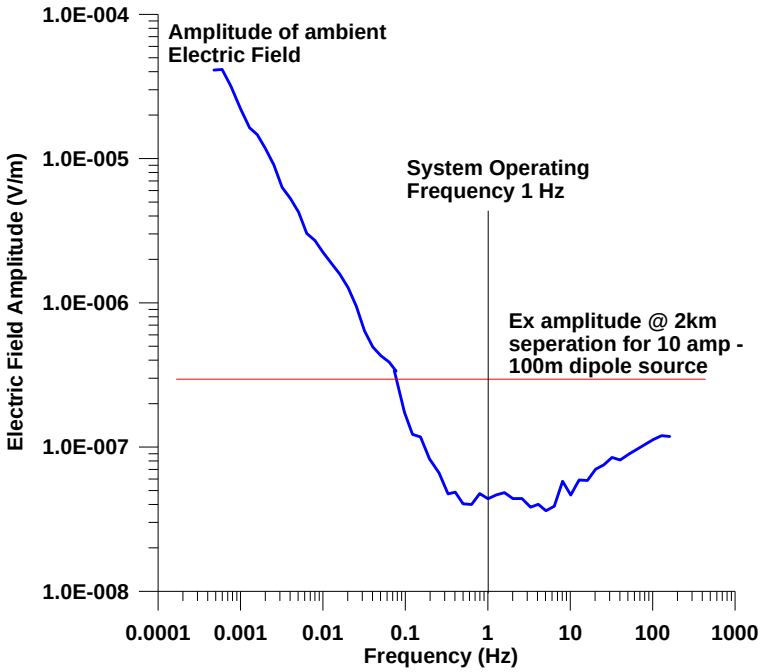

Figure 28. Amplitude of naturally occurring electric field as a function of frequency (Gasperikova et al. 2003), that would be considered noise to that electromagnetic system considered here for monitoring, shown as blue curve. The horizontal red line represents the signal amplitude at a source-receiver separation of 2 km at an operating frequency of 1 Hz for a 100 m electric dipole energized with 10 A of current.

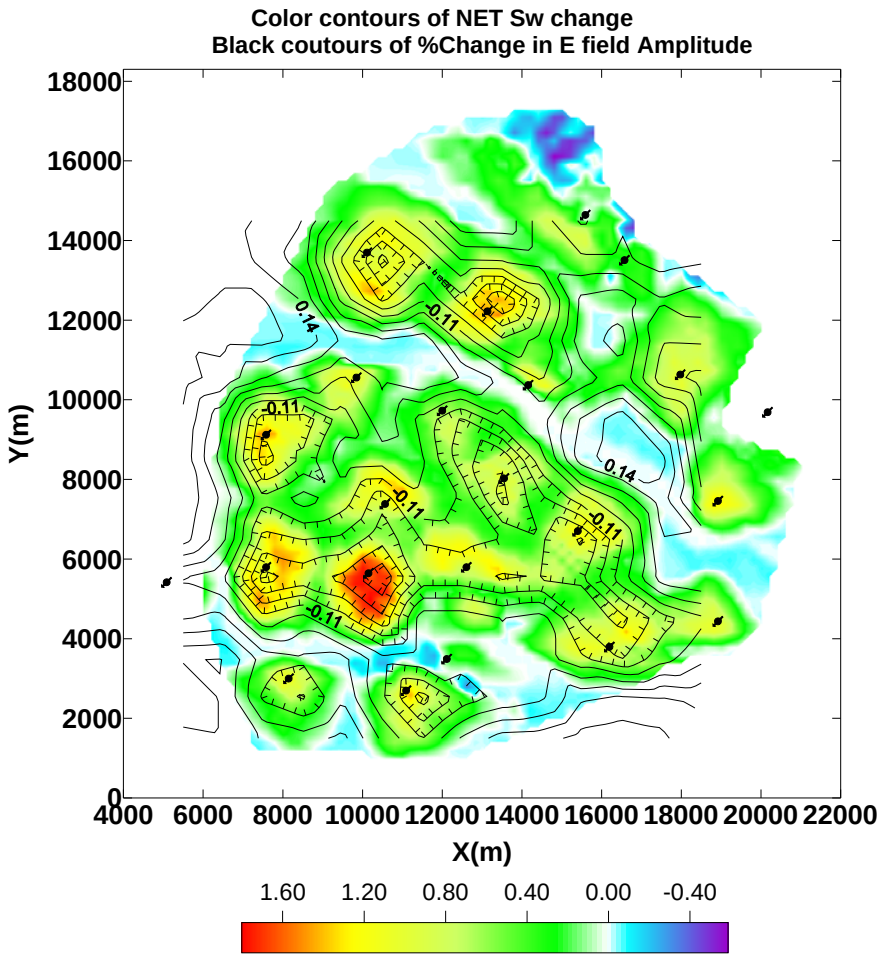

Figure 29. Color contours of the net change in water saturation over the vertical interval of the reservoir between 2020 and initial conditions. The change in the amplitude of the electric field from an electric dipole source at a separation of 2 km is overlaid as black contours. The peak-to-peak change is electric field amplitude is 1.2 %. Note the direct correlation between decreases in the electric field amplitude and increases in water saturation (decreased electric resistivity of the reservoir). Locations of injection wells are shown by black circles with arrows through them.

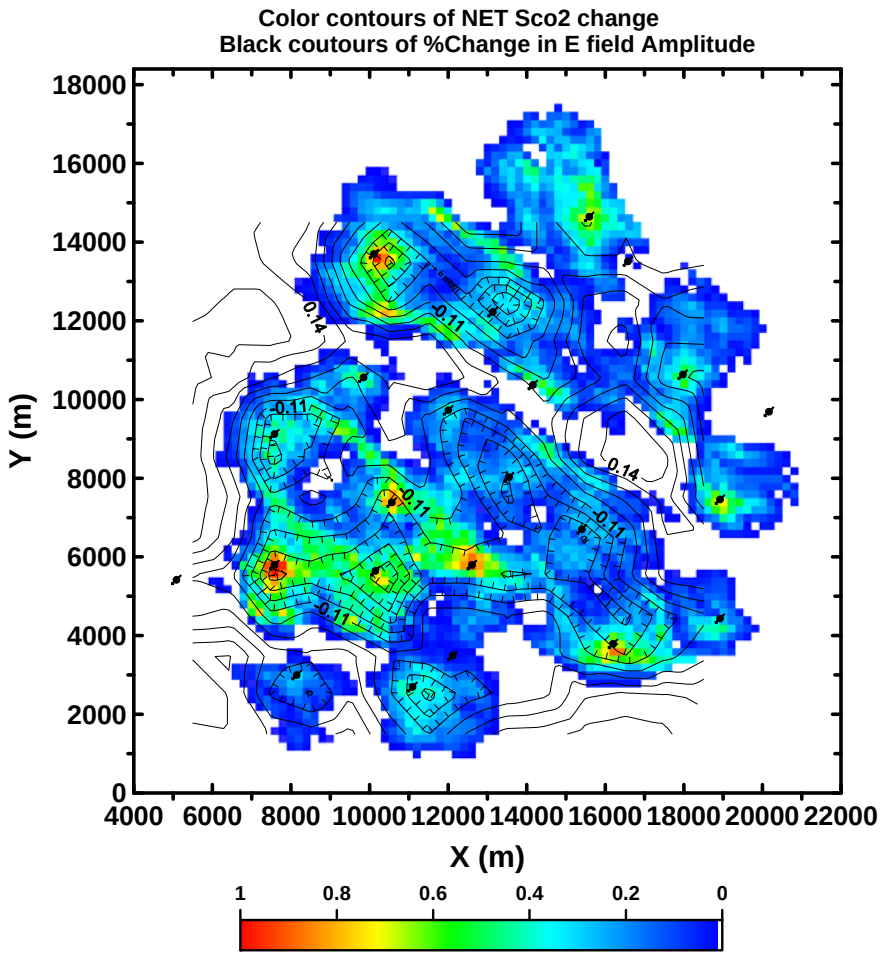

Figure 30. Color contours of the net change in CO_2 saturation (ΔS_{CO2}) over the vertical interval of the reservoir between 2020 and initial conditions. The change in the amplitude of the electric field from an electric dipole source at a separation of 2 km is overlaid as black contours. The peak-to-peak change is electric field amplitude is 1.2 %. Location of injection wells are shown by black circles with arrows through them.

On-shore EGR project - Rio Vista Gas Field, California

It is natural to consider geophysical techniques for monitoring of CO_2 movement within hydrocarbon reservoirs whether the CO_2 is introduced for enhance oil/gas recovery or for geologic sequestration because of the large body of experience in their application in the petroleum industry. Among geophysical techniques, seismic methods are by far the most highly developed. Due to cost considerations, other less expensive techniques are being considered for monitoring. This part of the report considers the use of surface gravity and seismic as a means of monitoring the movement of CO_2 within a gas reservoir.

The applicability of geophysical techniques depends, first, on the magnitude of the change in the measured geophysical property produced by CO_2, and second, on the inherent resolution of the technique. Finally, the applicability also depends on the configuration in which the measurement is deployed.

Gravity methods sense changes in density, and seismic methods depend on both density and elastic stiffness. These physical properties are known for CO_2, typical reservoir fluids, and their mixtures (Batzle and Wang, 1992; Magee and Hawley, 1994, NIST, 1992) so assessments can be made of expected changes in geophysical properties.

Rock Properties Model

One of the scenarios we have studied was a gas field that in general resembles conditions of the Rio Vista reservoir in Sacramento Basin. The field size is about 15 km x 15 km. The zone of interest is at about 1,300 m depth. The unit is of the Eocene age and it is called the Domengine sand. The average thickness of the reservoir is about 50 m. Contacts with the underlying Capay shale and overlying Nortonville shale are conformable (Johnson, 1990). The unit consists of series of interbedded marine sands

and shales, with sand being a predominant lithology. The Domengine sand is poorly consolidated.

We have used a reservoir simulation (Oldenburg et al., 2004) where the CO_2 injection well is in the center of the field and four production CH_4 wells are at the corners about 800 m away from the injection well (Figure 31b). This is only one five-spot simulation domain; there are 25 CO_2 injection wells, and 16 CH_4 production wells, and 8 monitoring wells placed over the central part of the gas field (Oldenburg et al., 2004) as shown in Figure 31a. CO_2 injection begins at the base of the 50 m thick reservoir interval. The porosity is 0.30, permeability is 10^{-12} m^2 (1 Darcy), residual brine saturation is 0.20, and reservoir temperature is 75° C. Reservoir pressure at the start of CO_2 injection is 5 MPa, and at the end of the last simulation (15 years) is 6 MPa. CH_4 density is 29.0 kg/m^3 at pressure of 5.0 MPa and temperature of 75° C. The density of CO_2 under the same conditions is 90.5 kg/m^3. The CO_2 injection rate is 3 kg/s (260 t/day) and CH_4 production rate is 0.56 kg/s (48 t/day).

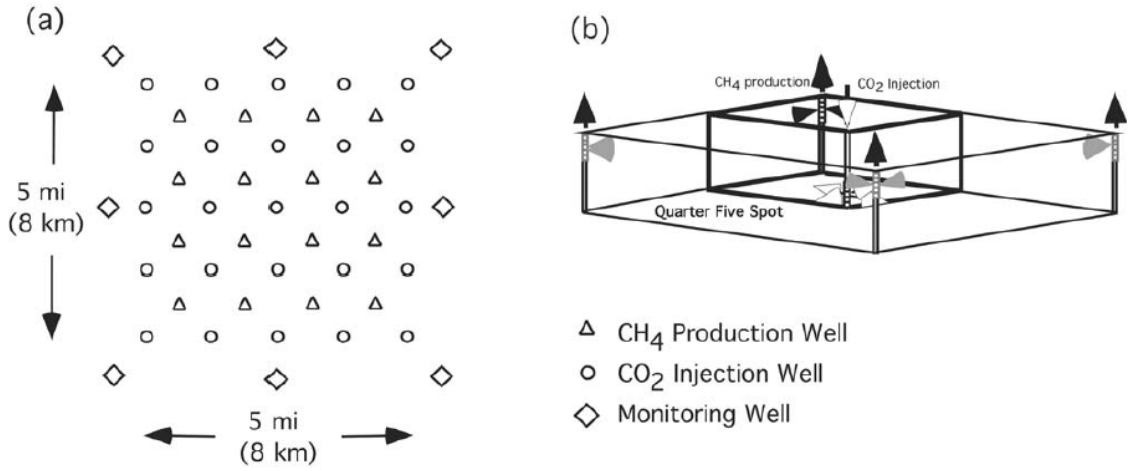

Figure 31: (a) Schematic of well pattern for CO_2 sequestration/enhanced gas recovery simulation with well spacing of 1.6 km, (b) Perspective view of quarter five-spot simulation domain (after Oldenburg et al., 2004).

The properties (density and bulk modulus) of the CO_2 are calculated assuming hydrostatic pressure and a temperature at 1,300 m of 75°C using the NIST14 code (Magee and Howley, 1994). The bulk rock density D_{bulk} of the reservoir is calculated using;

$$D_{bulk} = (1 - S_w - S_{CO_2})D_{grain} + S_w D_{brine} + S_{CO_2} D_{CO_2} \quad (1)$$

where, S_w is the brine saturation, S_{CO2} is the CO_2 saturation, D_{grain} is the grain density, D_{brine} is the brine density and D_{CO2} is the CO_2 density. The density effect of CO_2 dissolved in the brine is neglected. Quartz sand grains (D_{grain} = 2650 kg/m^3) are assumed.

Four time steps were considered – initial conditions, 5 years, 10 years and 15 years into the CO_2 injection. Using these flow simulations, geophysical models were created to study the gravity and seismic methods responses to changes in the reservoir due to the CO_2 injection.

Figure 32 is a plane view of CO_2 saturation in the reservoir at the depth of 1,325 m after 10 years of CO_2 injection. The CO_2 injection well is at (0,0) and CH_4 production wells are at the corners of the grid: (-800, -800), (800, -800), (-800, 800), and (800, 800).

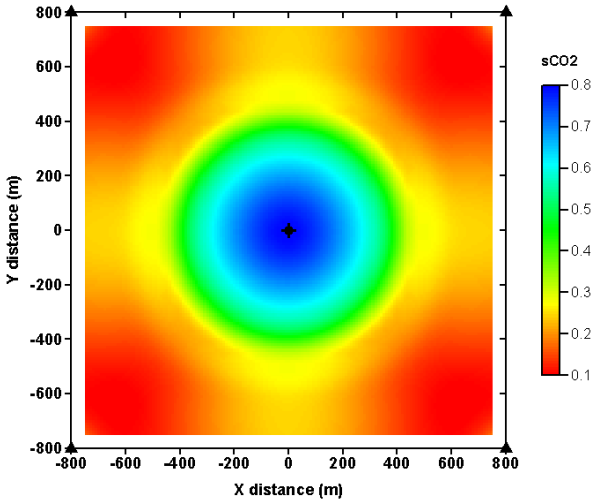

Figure 32: Plan view of CO_2 saturation at the depth of 1,325 m as a function of x and y coordinates after 10 years of injection.

Figure 33 is a cross-section of CO_2 saturation through the center of the reservoir after 10 years of CO_2 injection. The injector is at the bottom of the reservoir (depth of 1,350 m) at x = 0 m.

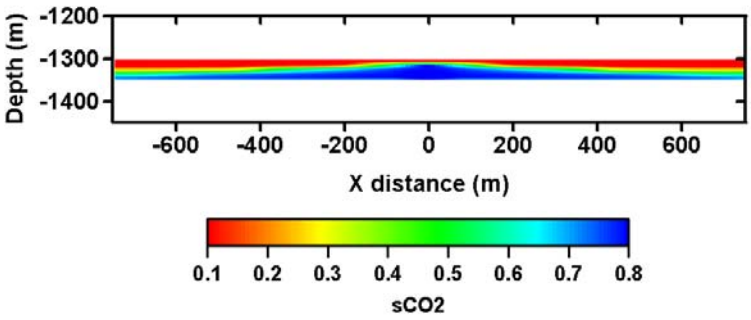

Figure 33: A cross-section of CO_2 saturation in the center of the reservoir after 10 years of CO_2 injection as a function of depth and horizontal position.

Figures 34 - 36 respectively are cross-sections of Vp-velocity, Vs-velocity, and density through the center of the reservoir after 10 years of CO_2 injection. All these figures indicate a symmetric pattern between the injection and production wells and relatively small changes both in velocity and density.

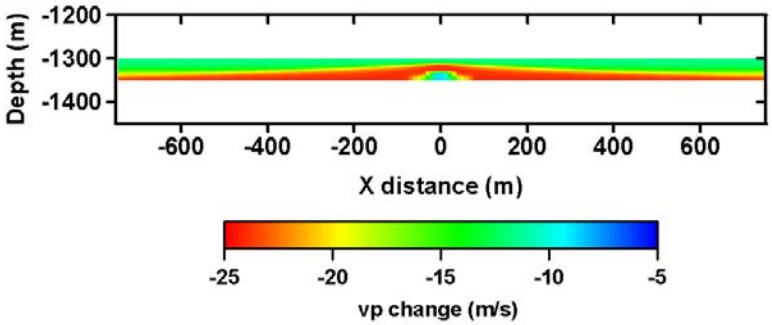

Figure 34: Vp-velocity change between initial conditions and 10 years into the CO_2 injection as a function of depth and horizontal position.

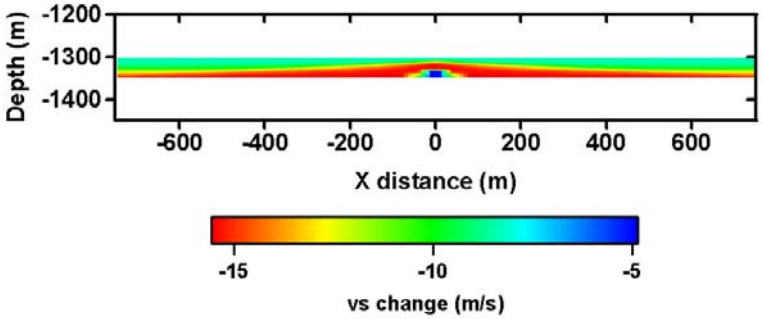

Figure 35: Vs-velocity change between initial conditions and 10 years into the CO_2 injection as a function of depth and horizontal position.

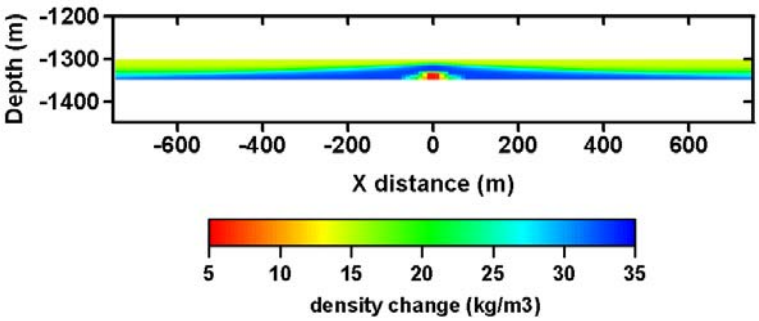

Figure 36: Density change between initial conditions and 10 years into the CO_2 injection as a function of depth and horizontal position.

Gravity modeling and inversion

The vertical component of the surface gravity response of the model after 5 years, 10 years, and 15 years of CO_2 injection is shown in Figures 37, 38, and 39, respectively. CO_2 has higher density than CH_4 under reservoir conditions and therefore by injecting CO_2 into the reservoir density increases which in turn causes an increase in the gravity response. The peak surface gravity response is about 2 μGal, 3.5 μGal, and 5 μGal after 5, 10 and 15 years of injection. Signals for 5 and 10 years are very close to the limits of current survey technologies and might not be measurable in the field. The response after 15 years of CO_2 injection should be measurable in the field. Brown et al. (2002) reported repeatability of 3.5 μGal for a gravity survey at Prudhoe Bay, Alaska. Nooner et al. (2003) reported repeatability of 2.5 μGal and a detection threshold for time-lapse changes of 5 μGal for a time-lapse gravity survey of the Sleipner CO_2 sequestration site in the North Sea.

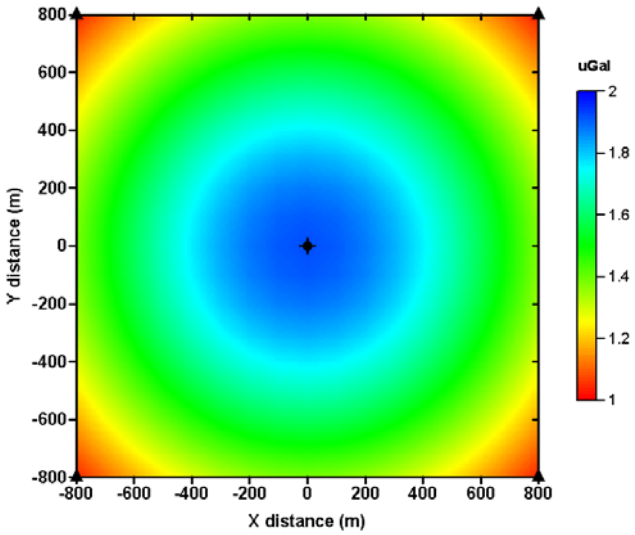

Figure 37: Vertical component of the surface gravity response of the model after 5 years of CO_2 injection as a function of x and y coordinates.

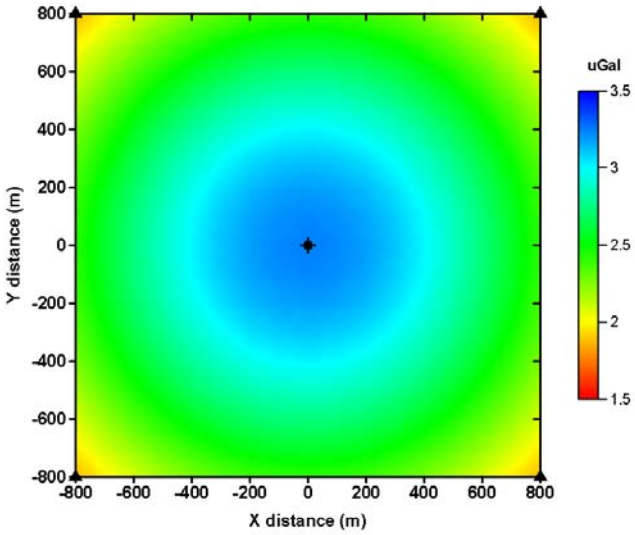

Figure 38: Vertical component of the surface gravity response of the model after 10 years of CO_2 injection as a function of x and y coordinates.

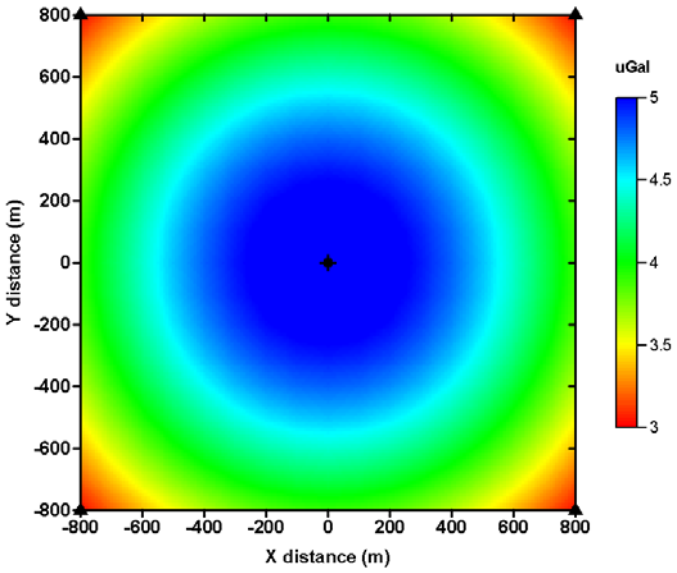

Figure 39: Vertical component of the surface gravity response of the model after 15 years of CO_2 injection as a function of x and y coordinates.

The inversion of gravity data is very important since construction of density contrast models significantly increases the amount of information that can be extracted from the gravity data. However, a principal difficulty with the inversion of the gravity data is the inherent non-uniqueness and that there is no inherent depth resolution. This difficulty can be overcome by introduction of prior information. Some authors prescribe the density variations and invert for the geometrical parameters of the model (e.g. Oldenburg, 1974), others assume a constant density contrast and invert for the position of a polyhedral body from isolated anomalies (e.g. Pedersen, 1979). Li and Oldenburg (1998) developed another approach, where gravity data is inverted directly by minimizing an objective function of the density model subject to fitting the observations. This approach incorporates also prior information via a reference model and depth weighting. We adopted Smith et al. (1999) approach described for magnetotelluric data inversion, in which the top and base of the reservoir is known and we invert for a density variation inside of the reservoir. The inversion result is a cumulative density change in the reservoir as a function of x and y coordinates. Because the model space and inversion domain space can be different, one needs to calculate a parameter that is equal in both of these domains, a product of a cumulative cell density change and its volume, in order to compare inversion results with a true model.

The gravity inversions of the vertical component of the surface gravity response for each time are shown in Figures 40, 41, and 42 respectively.

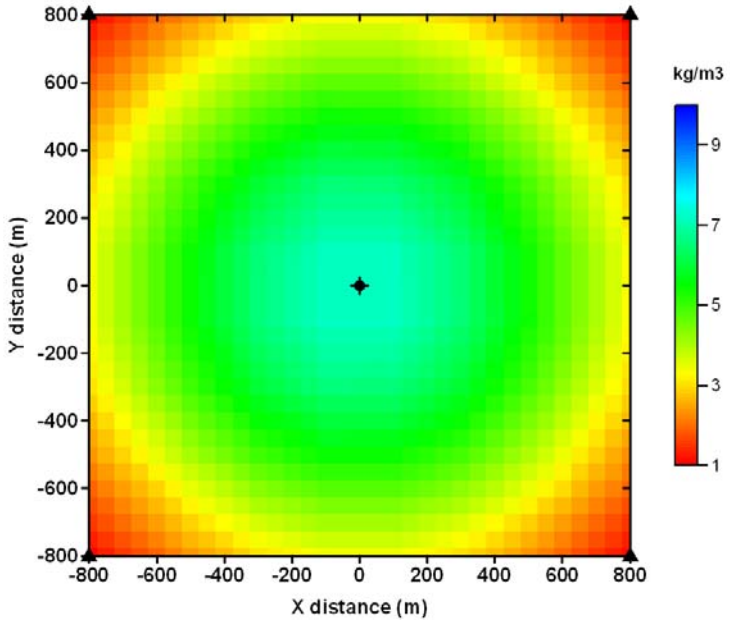

Figure 40: Density change (in kg/m^3) recovered by inversion of the vertical component of the surface gravity response of the model after 5 years of CO_2 injection as a function of x and y coordinates.

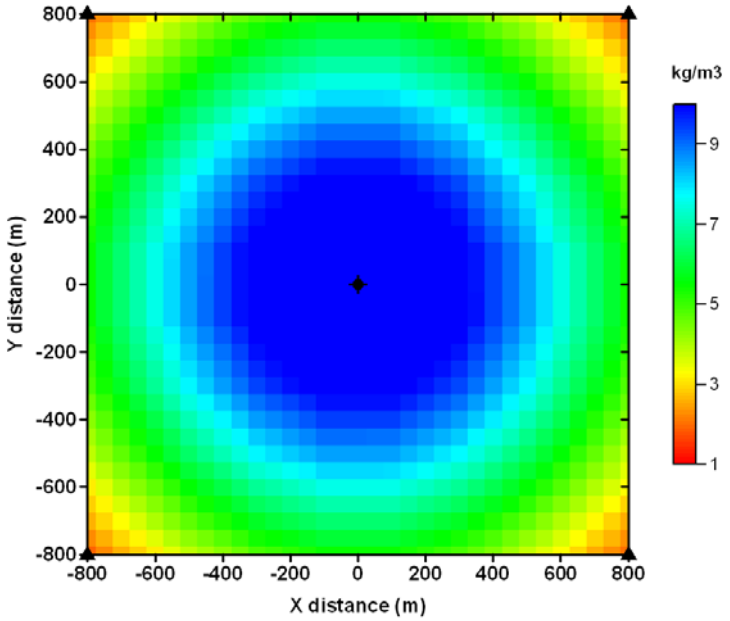

Figure 41: Density change (in kg/m^3) recovered by inversion of the vertical component of the surface gravity response of the model after 10 years of CO_2 injection as a function of x and y coordinates.

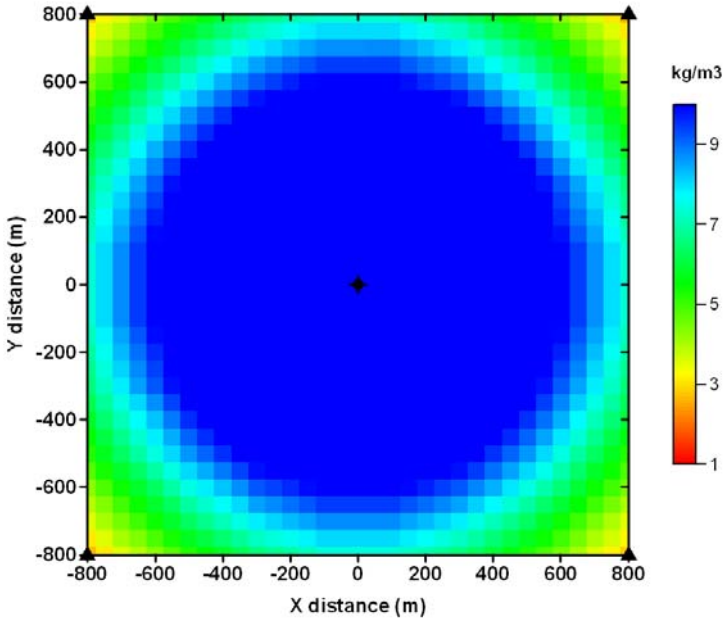

Figure 42: Density change (in kg/m^3) recovered by inversion of the vertical component of the surface gravity response of the model after 15 years of CO_2 injection as a function of x and y coordinates.

Figures 40, 41, and 42 show that CO_2 is replacing CH_4 further and further from the injection well (0, 0) with time and therefore the CO_2 - CH_4 contact moves away from the injection well. Since the five-point simulation area is centered over the CO_2 injection well and CH_4 production wells contributed only partially, the gravity high is centered on the injection well. To evaluate how much change in the response is due to one injection well (0,0) and one production well (800,800) we modified the model after 15 years of CO_2 injection to reflect that, and the gravity response of this model is shown in Figure 43. Figure 44 shows the inversion results for this model overlaid on the true density model. The gravity inversion used in this study is solving for density changes between the top and bottom of the reservoir. The inversion result is a cumulative density change in the reservoir as a function of x and y coordinates. Because the model space and inversion domain space are different, in order to compare inversion results with a true model, we need to calculate a parameter that is equal in both of these domains, and that is a product of a cumulative cell density change and its volume. The true model is displayed in color, and the inversion

results are displayed as red contours. The true model shows that density near the injection well is higher than near the production well. The inversion finds a broad smooth anomaly centered between the injection and production wells.

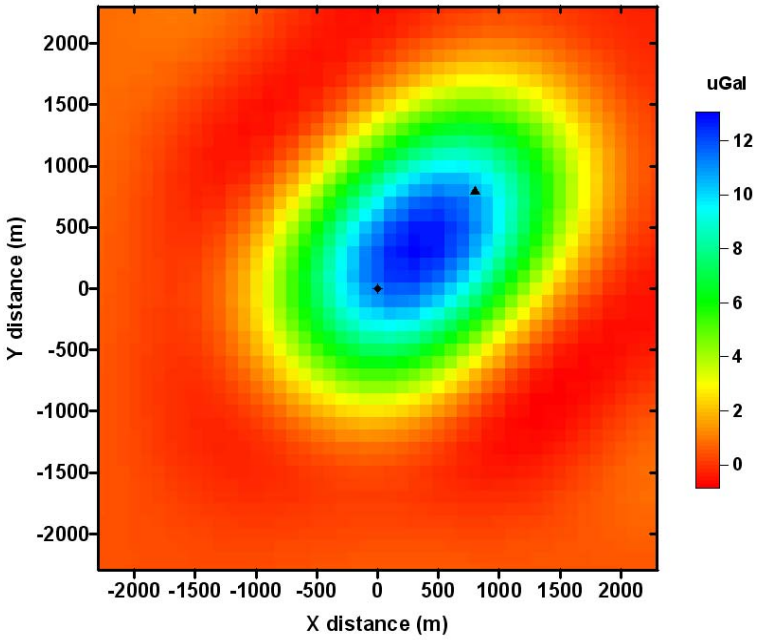

Figure 43: Vertical component of the surface gravity response of a modified model after 15 years of CO_2 injection with an injection well at (0,0) and a production well at (800,800) as a function of x and y coordinates.

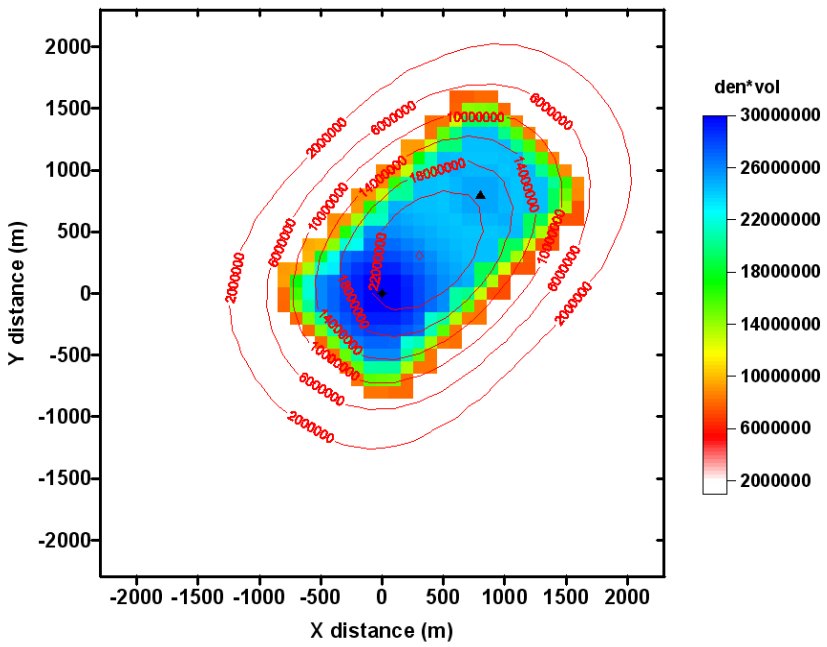

Figure 44: True density model overlaid by contours of the inversion results as a function of x and y coordinates.

Seismic modeling

NMO CDP stack sections of the model after 5 years, 10 years, and 15 years of CO_2 injection are shown in Figures 45, 46, and 47 respectively. Reservoir produces weak anomalies associated with the changes in CO_2 saturation. Seismic velocities change only 1–2 %. The seismic amplitudes are small and therefore seismic is not a reliable monitoring tool of CO_2 movement under present reservoir conditions.

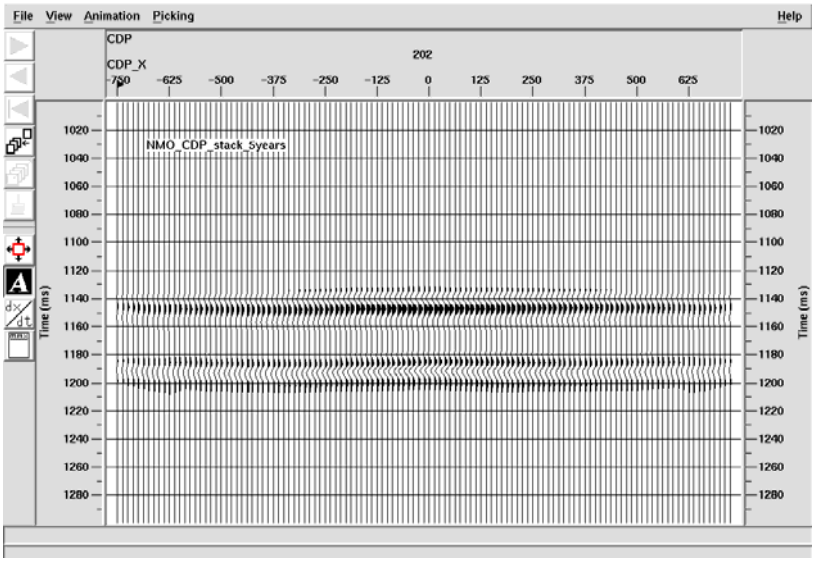

Figure 45: NMO CDP stacked section of the model after 5 years of CO_2 injection.

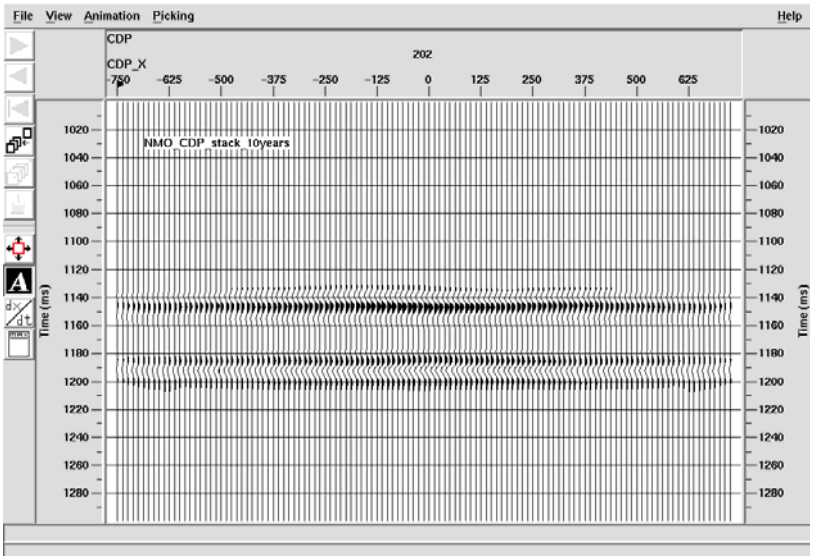

Figure 46: NMO CDP stacked section of the model after 10 years of CO_2 injection.

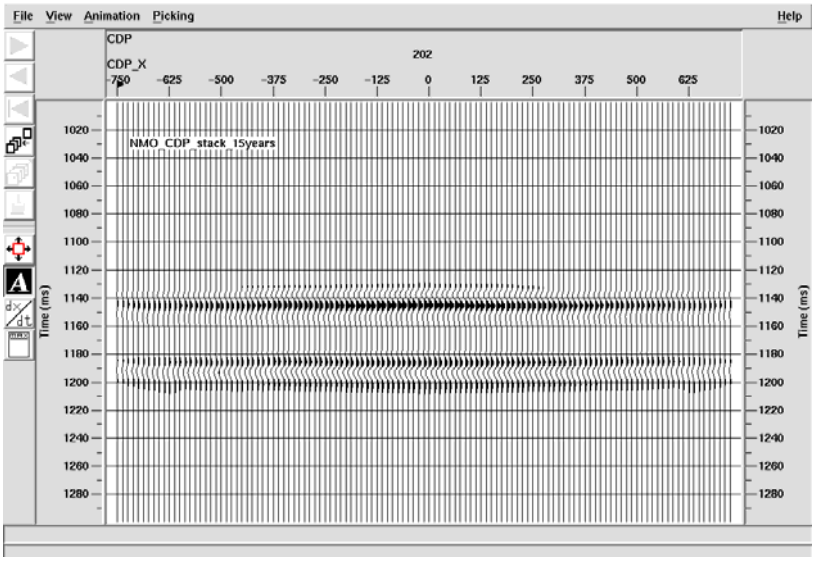

Figure 47: NMO CDP stacked section of the model after 15 years of CO_2 injection.

Figure 48 shows the NMO section as function of offset centered 300 m away from the injection well for the model after 10 years of CO_2 injection. Figure 49 shows amplitude at the top of the reservoir at the same location (x=-300 m), as a function of offset after 5, 10, and 15 years of CO_2 injection. There is less than a 2% change for models after 5 and 10 years of CO_2 injection, and about 3% for model after 15 years of CO_2 injection. Figure 50 shows predicted Rpp amplitude as a function of offset for the reservoir properties used in this study. All three figures (Figures 48-50) confirm that the change in the amplitude as a function of offset is on the edge of detectability to be able to predict the CO_2 saturation from AVO measurements for this model. Assuming normal S/N ratios and changes present over many traces, 2-5% change both in amplitude and AVO should be detectable in the field data (Daley, personal communication).

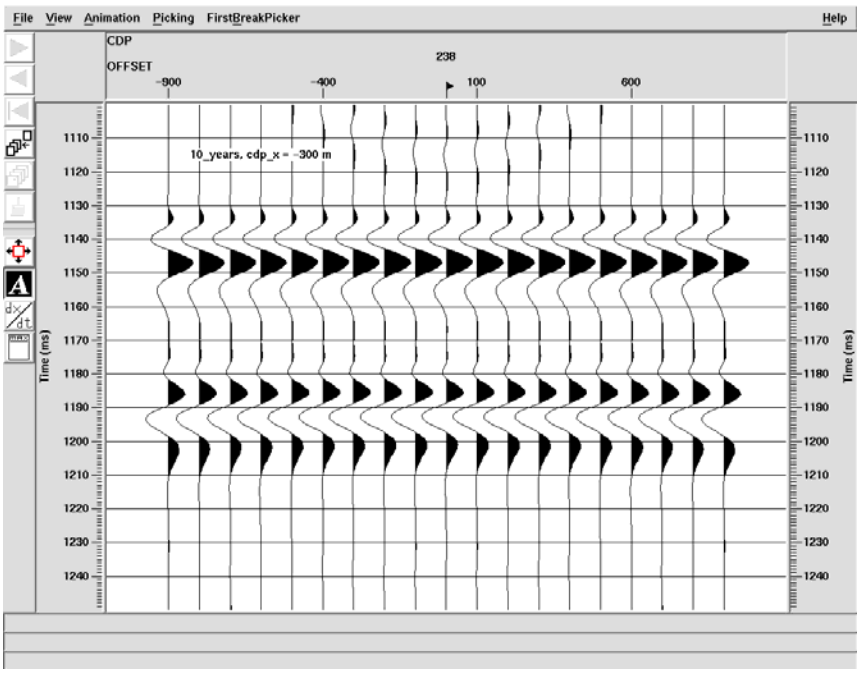

Figure 48: NMO section for CDP 238 (x = -300 m) showing seismic amplitude as a function of offset of model after 10 years of CO_2 injection.

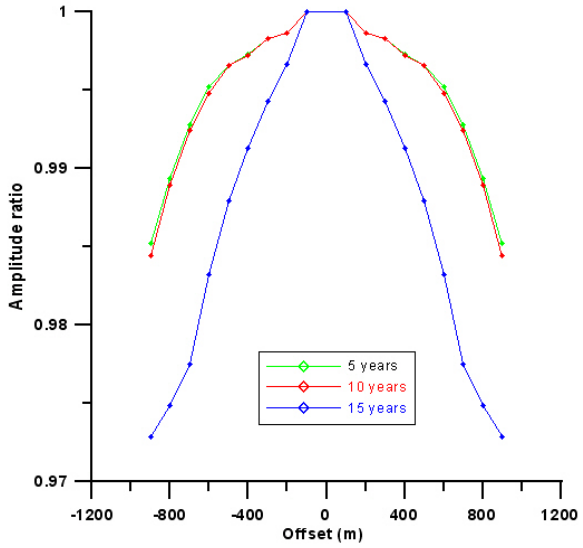

Figure 49: AVO amplitude ratio as a function of offset for CDP 238, which is 300 m away from the injection well.

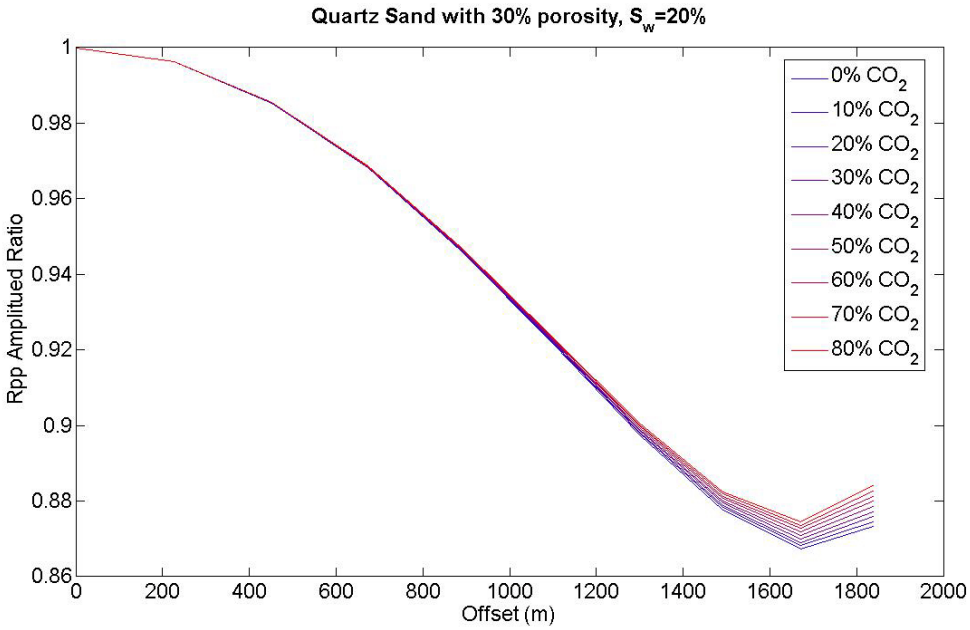

Figure 50: Model AVO results – Rpp amplitude as a function of offset for quartz sand of 30% porosity and 20% water saturation.

Ventura Oil Field

The Ventura Field is located in the center of the Venture Basin, 65 miles west and north of Los Angeles. The basin is filled with tertiary sediments. The Pliocene section is about 6,000 m thick and outcrops within the Ventura Field. This section of deep-water fan sediments consists of many interbeded sandstones and shales. Mid Pleistocene stresses compressed the basin, folded the sediments and formed complexly faulted, asymmetric structure, the east-west trending Ventura Anticline. The Ventura Field produces from Pliocene unit at depths of 1,000 to over 4,000 m. Five major fault blocks A, B, C, D, and N have been identified during development. The blocks B, C, and D between 1,500 m and 3,000 m are candidates for CO_2 sequestration.

Using average reservoir properties we calculated a response in seismic amplitude (Figure 51) and density change (Figure 52) due to the change in CO_2 saturation. The values used in

these calculations are: depth to the top of the reservoir = 2,500 m, porosity = 14%, reservoir temperature = 87.8° C, reservoir pressure = 22 MPa, GOR ~ 100 l/l, oil gravity = 30° API, water saturation = 0.6, oil saturation = 0.4.

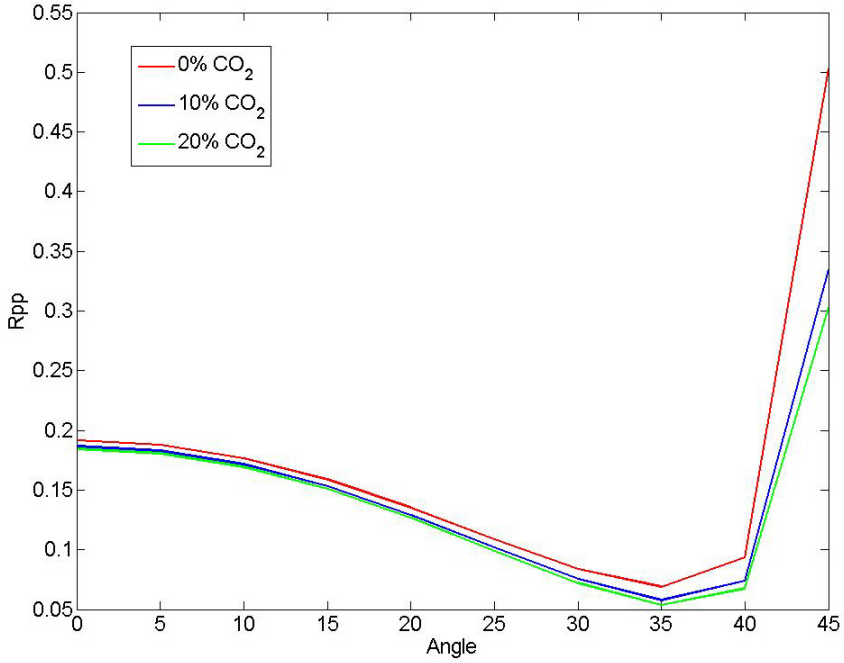

Figure 51: Seismic amplitude as a function of angle (offset) for a hypothetical model for Ventura oil field.

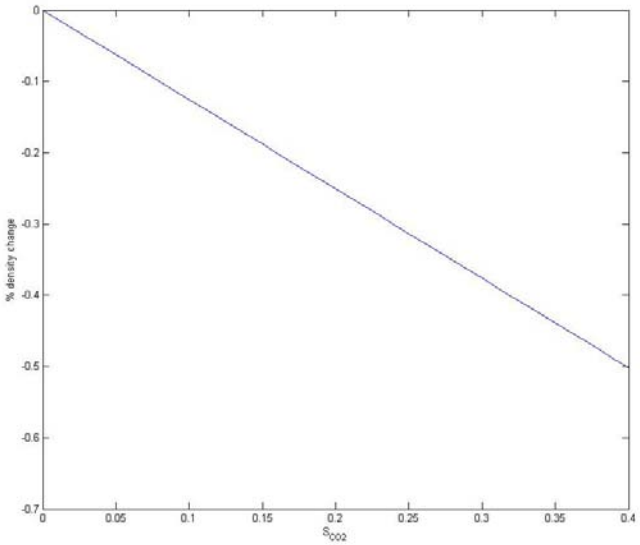

Figure 52: Density change due to a change in CO_2 saturation for a hypothetical model for Ventura oil field.

Based on the signal levels in Figures 51 and 52 neither the seismic nor gravity methods would be able to monitor changes in the reservoir due to CO_2 saturation change for conditions used in this hypothetical model.

Results and Discussion

The difference in the vertical component of gravity (G_z) on the surface caused by CO_2 injection over a 20-year period for the Schrader Bluff model is on the order of 2 μGal, which is in the noise level of the field survey (Hare, 1999). The negative change in the response is caused by increased CO_2 saturations reducing the bulk density of the reservoir. The spatial variations in the changes in G_z as well as the vertical gradient of the vertical component of gravity (dG_z/dz) directly correlate with the spatial variations in the net density changes within the reservoir. Again, the magnitude of the signal measured in the field (2–10 EU) is above the gradiometer accuracy (0.5–1 EU), but the difference between initial conditions and 20 years into CO_2 injection is very small (~0.1 EU). If the noise levels of measurements of the changes in dG_z/dz could be reduced by permanent sensor emplacement and continuous monitoring gravity and gradient measurements may offer a tool for monitoring.

Borehole measurements of gravity just above the reservoir do produce measurable change in the vertical component of gravity that could be used to map lateral distributions of injected CO_2. The changes in dG_z/dz measured in the borehole are below the ability of current technology to distinguish. However, current work on borehole gravity tools may change this situation within the next few years. The difference in both the borehole gravity response and the vertical gravity gradient (dG_z/dz) measured in vertical profiles within boreholes clearly identifies the position of the reservoir. The sign of the change reflects the changes in the local densities caused by either water or CO_2.

There is a clear change in seismic amplitude associated with the reservoir caused by the changes is water and CO_2 saturation. In addition, there is a change in the seismic AVO effects. Both seismic amplitude and AVO can be exploited to make quantitative estimates of saturation changes. Forward calculations using Zoeppritz equation for both 2005 and 2020 models support this argument.

The electrical resistivity of reservoir rocks is highly sensitive to changes in water saturation. This high sensitivity to water saturation in a reservoir can be exploited by electromagnetic (EM) techniques where the response is a function of the electrical resistivity of the formation. Of all the possible combination of EM sources and measured EM fields one system combines both relative ease of deployment with high sensitivity to reservoirs of petroleum scale and depth. This technique uses a grounded electric dipole that is energized with an alternating current at a given frequency to produce time varying electric and magnetic fields that can be measured on the earth's surface. To simulate such an EM system we have calculated the electric field on the surface of the Schrader Bluff model using 100 m electric dipoles operating at 1 Hz an measuring the resulting electric field at a separation of 2 km in-line with the transmitting dipole. The generated electric field for the Schrader Bluff model, using only a small portable generator is an order of magnitude above the background electric field (noise) at the operating frequency of 1 Hz. This means that synchronous detection of the signal combined with stacking can recover signal variations to better than 1 percent. There is a direct one-to-one correspondence with the change in S_w and the change in the electric field amplitude. While this signal level is low, it can be measured give the signal-to-noise ratio of the data. While this represents a potential low-cost monitoring technique it is best suited for CO_2 – brine systems where there is a one-to-one correlation between the change in water saturation and the change in CO_2 saturation (since $S_w + S_{CO2} = 1$). In petroleum reservoir such as Schrader Bluff the presence of hydrocarbon as additional fluids eliminates the one-to-one correlation between changes in S_w and changes in S_{CO2}. This type of EM technique has not yet been employed as a monitoring tool within the petroleum industry. However, EM technology is currently the subject of a significant upsurge in industry

interest. Several commercial contractors are now offering this technique as a survey tool, most notably, in the offshore environment where it is currently being used as an exploration tools (Ellingsrud et al. 2002). The equipment and service providers exist to apply this technique for monitoring in the future.

For the gas field used in this study, the change in reservoir properties are very small and neither gravity nor seismic methods would provide information necessary for monitoring of CO_2 movement.

Not enough information was available to create a representative model of the Ventura oil field. Preliminary calculations using average reservoir properties suggest, however, that neither gravity nor seismic methods will be able to give information about CO_2 saturation change.

Conclusions

Both surface and borehole gravity measurements have been modeled for Schrader Bluff. The injection of CO_2 produces a bulk density decrease in the reservoir that in turn produces a reduction in the gravitation attraction from the reservoir. The spatial pattern of the change in the vertical component of gravity (G_z) as well as the vertical gradient of gravity (dG_z/dz) is directly correlated with the net change in density of the reservoir. The difference in G_z on the surface caused by CO_2 injection over a 20-year period is on the order of 2 μGal, which is below the level of repeatability of current field surveys (Hare, 1999). However, measurements made in boreholes just above the reservoir interval (1,200 m depth) are sensitive enough to observe measurable changes in G_z as CO_2 injection proceeds. Such measurements made in numerous wells could map the areas of net density changes caused by injected CO_2 and water within the reservoir. The time-lapse changes in the borehole G_z and dG_z/dz clearly identify the vertical section of the reservoir where fluid saturations are changing.

Model results show a clear change in seismic amplitude associated with the reservoir due to the changes in water and CO_2 saturation. Moreover, there is a change in the seismic AVO effects. Both seismic amplitude and AVO can be used to make quantitative estimates of saturation changes, subject to modeling assumptions.

The electrical resistivity of rocks is primarily a function of porosity and water saturation (S_w). When the porosity is known, or can reasonably be assumed to have small spatial variation, the changes in electrical resistivity are directly related to the changes in water saturation. EM techniques can be used to map such spatial variations in electrical resistivity. EM field system that combines relative ease of deployment with high sensitivity to petroleum reservoirs generated electric field for the Schrader Bluff model that was an order of magnitude above the background electric field (noise) at the operating frequency of 1 Hz. This means that synchronous detection of the signal combined with stacking can recover signal variations to better than 1 percent. The change in the electric field amplitude is directly proportional to the change in S_w. While this signal level is low, it can be measured given the signal-to-noise ratio of the data. This potential low-cost monitoring technique is best suited for CO_2 – brine systems where there is a one-to-one correlation between the change in water saturation and the change in CO_2 saturation. In petroleum reservoirs such as Schrader Bluff, the presence of hydrocarbons as additional fluids eliminates this one-to-one correlation.

Because the changes in reservoir properties for the gas field used in this study are very small neither gravity nor seismic methods would provide information necessary for monitoring of CO_2 movement.

Not enough information was available to create a representative model of the Ventura oil field. Preliminary calculations using average reservoir properties suggest, however, that neither gravity nor seismic methods will be able to give information about CO_2 saturation change.

Acknowledgments

This work was conducted as part of the WESTCARB project, supported by the Assistant Secretary for Fossil Energy, Office of Sequestration, Hydrogen, and Clean Coal Fuels, through the National Energy Technology Laboratory, U.S. Department of Energy, under Contract No. DE-AC02-05CH11231.

REFERENCES

Archie, G. E., 1942, The electrical resistivity log as an aid in determining some reservoir characteristics: Trans., AIME 146, pp. 54-62.

Batzle, M., and Wang, Z., 1992, Seismic properties of pore fluids, Geophysics, **57**, pp. 1396-1408.

Brown, J.M., Klopping, F.J., van Westrum, D., Niebauer, T.M., Billson, R., Brady, J., Ferguson, J., Chen, T., and Siebert, J., 2002, Preliminary absolute gravity survey results from water injection monitoring program at Prudhoe Bay: Proceedings from SEG International Exposition 2002, 791-793.

Castagna, J.P, Swan, H. W., Forster, J.F., 1998, Framework for AVO gradient and intercept interpretation, Geophysics, **63**, pp. 948-956.

Dvorkin, J. and Nur, A., 1996, Elasticity of high-porosity sandstones: Theory of two North Sea data sets: Geophysics, **61,** pp. 1363-1370.

Ellingsrud, S., Eidesmo, T., Johansen, S., Sinha, M.C., MacGregor, L. M., Constable, S., 2002, Remote sensing of hydrocarbon layers by seabed logging (SBL): Results from a cruise offshore Angola: The Leading Edge, **21**, pp. 972-982.

Gasperikova, E., Hoversten, G.M., Ryan, M.P., Kauahikaua, J.P., Newman, G.A., and Cuevas, N., 2003, Magnetotelluric investigations of Kilauea volcano, Hawai'i. Part I: Experiment design and data processing. Journal of Geophysical Research, in review.

Hare, J.L., Ferguson, J.F., and Aiken, C.L.V., 1999, The 4-D microgravity method for waterflood surveillance: Amodel study from the Prudhoe Bay reservoir, Alaska: Geophysics, **64**, 78-87.

Hill, G., B. Moore, and M. Weggeland, 2000, The CO_2 Capture Joint Industry Project, in Proceedings of the Fifth International Conference on Greenhouse Gas Control Technologies, D. Williams, B. Durie, P McMullan, C. Paulson, and A. Smith, eds., CSIRO, Collingwood, Victoria, Australia, pp. 248-253.

Hoversten, G., M., Gritto, R., Washbourne, J., Daley, T., M., 2003, Pressure and Fluid Saturation Prediction in a Multicomponent Reservoir, using Combined Seismic and Electromagnetic Imaging. Geophysics, (in press Sept-Oct 2003).

Johnson, D. S., 1990, Rio Vista Gas Field – U.S.A., Sacramento Basin, California: in Structural Traps III: Tectonic Fold and Fault Traps Dane S. Johnson 1990 AAPG Special Publication , Pages 243 - 263.

Landro, M., 2001, Discrimination between pressure and fluid saturation changes from time-lapse seismic data: Geophysics, **66**, pp. 836-844.

Li, Y., and Oldenburg, D.W., 1998, 3-D inversion of gravity data: Geophysics, **63**, p. 109-119.

Magee, J. W., and Howley, J. A., 1994, Gas Processors Association, Tulsa, OK Research Report, RR-136.

NIST Mixture Property Database, 1992, U.S. Department of Commerce, National Institute of Standards and Technology, Standard Reference Data Program, Gaithersburg, MD 20899.

Nooner, S.L., Zumberge, M.A., Eiken, O., Stenvold, T., and Sasagawa, G.S., 2003, Seafloor micro-gravity survey of the Sleipner CO2 sequestration site, EOS Trans. AGU, **84**(46), Fall Meet. Suppl., Abstract GC31A-01.

Oldenburg, C.M., Stevens, S.H., and Benson, S.M., 2004, Economic feasibility of carbon sequestration with enhanced gas recovery (CSEGR): Energy, **29**, p. 1413-1422.

Oldenburg, D.W., 1974, The inversion and interpretation of gravity anomalies, Geophysics, **39**, p. 394-408.

Pedersen, L.B., 1979, Constrained inversion of potential field data: Geophysical Prospecting, **27**, p. 726-748.

Popta, J.V., Heywood, J.M.T., Adams, S.J., and Bostock, D.R., 1990, Use of borehole gravimetry for reservoir characterization and fluid saturation monitoring: SPE 20896, p. 151- 160.

Shuey, 1985, A simplification of the Zoeppritz equations: Geophysics, **50**, pp. 609-614.

Smith, J.T., Hoversten, G.M., Gasperikova, E., Morrison, H.F., 1999, Sharp boundary inversion of 2-D magnetotelluric data: Geophysical Prospecting, **47**, p. 469-486.

Thomsen L.A., Brady J.L., Biegert E., Strack K.M., 2003, A Novel Approach to 4D Full Field Density Monitoring, SEG workshop.